universität wien

MASTERARBEIT

"1,4-Disubstituted 1,2,3-triazoles as novel ligand scaffold for the development of organometallic anticancer agents"

Verfasst von

Christoph Riedl B.Sc.

Angestrebter akademischer Grad

Master of Science (M.Sc.)

Wien, 2015

Studienkennzahl lt. Studienblatt:	A 066 862
Studienrichtung lt. Studienblatt:	Masterstudium Chemie
Betreut von:	O. Univ.-Prof. Dr. Dr. Bernhard K. Keppler

ACKNOWLEDGEMENTS

I would like to thank

My supervisor O. Univ.-Prof. Dr. Dr. Bernhard K. Keppler for the opportunity to work in his group.

DI Dr. Wolfgang Kandioller for continuous encouragement throughout my thesis.

The NMR service team (Doris Höfer M.Sc., Dipl.-Chem. Dr. Paul-Steffen Kuhn, Josef Mayr M.Sc., DI Melanie Schmidlehner, Dipl.-Chem. Nadine Sommerfeld, and Ao. Univ.-Prof. Dr. Markus Galanski) for measurement of NMR spectra.

Ao. Univ.-Prof. Dr. Vladimir Arion and Dipl.-Ing. (FH) Alexander Roller for x-ray diffraction data collection and structure refinement.

The staff of the Core Facility for Mass Spectrometry and the Microanalytical Laboratory of the University of Vienna for measurement of mass spectra and elemental analyses.

My laboratory colleagues Dipl.-Chem. Britta Fischer, Carmen Hackl M.Sc., Stephan Mokesch M.Sc., and DI Melanie Schmidlehner for the constructive and pleasant work atmosphere.

Mag. Elfriede Limberger, Sylwia Kur B.Sc. and Ing. Norbert Kandler for their help with administrative and technical matters.

All the members of the working group for the unforgettable time spent during my master thesis. Special thanks go to Melanie for the measurement of countless 2D NMR spectra and Stephan for his help with ESI-MS investigations.

My colleagues and friends Alanca, Christian, Kathi, Kerstin, Lukas, Martin, and Max for mutual support and non-chemical diversion during our studies together.

Laura, Sebastian, and Valentin for being the best friends one could wish for.

My mother, father, and entire family for their unwavering support and encouragement throughout my entire life.

ABSTRACT

Platinum-based antineoplastic agents have been the chemotherapeutic treatment of choice over the last 20 years for a variety of cancerous growths. Nevertheless, they induce a number of severe side effects, possess a limited scope of treatable tumors and several cancer types exhibit acquired or intrinsic resistances. Ruthenium(III) complexes have emerged as promising candidates for the development of improved anticancer agents with novel mode of action, higher selectivity, and increased range of treatable cancers. The first-in-class ruthenium(III) compound NKP-1339 (IT-139) has shown promising results in clinical trials. This metallodrug is thought to act as prodrug and undergo activation by reduction of the metal center under the hypoxic conditions of the tumor tissue. Interaction with the cytosolic protein GRP78 and the induction of oxidative stress caused due to redox activity of the metal center are thought to be responsible for the *in vivo* activity. Organometallic ruthenium(II) complexes have been thoroughly investigated for their antiproliferative potential, affording several exciting compounds, which are currently in an advanced preclinical stage. One promising approach for the development of organometallic anticancer agents is the coordination of bioactive molecules to the metal-arene fragment, yielding compounds able to interact with several different cellular targets and therefore with novel modes of action.

1,2,3-Triazoles have been shown to possess highly interesting biological features and are a motif present in numerous medicinal agents currently under preclinical evaluation. They can be synthesized in a straight-forward manner by copper(I)-catalyzed Huisgen 1,3-dipolar cycloaddition, also known as Click Chemistry. 4-Phenyl-substituted 1,2,3-triazoles are potential *N,C* chelates and may coordinate to different metal ions. However, the coordination chemistry and biological potential of the derived organometallic arene complexes is nearly unexplored. Over the course of this master thesis, six phenyl triazoles with different functional groups in position 1 were synthesized by copper(I)-catalyzed alkyne-azide cycloaddition. The obtained ligands were coordinated to a ruthenium(II) arene precursor as proof of concept for the *N,C*-coordination of 1,2,3-triazoles to metal arene complexes. The corresponding “piano-stool” configured complexes featuring chloride leaving group were successfully synthesized and isolated in elemental analysis purity. The ligands and organometallic compounds were characterized by 1D and 2D NMR spectroscopy, HR-MS, elemental analysis, solubility measurements, and single crystal x-ray diffraction where possible. Investigations on the behavior in aqueous solution and reactivity toward biomolecules via ESI-MS methods were performed to evaluate the suitability of the novel complexes as potential anticancer agents.

ZUSAMMENFASSUNG

Antineoplastische Medikamente basierend auf Platin sind seit Jahren die chemotherapeutische Behandlungsmethode der Wahl für eine Vielzahl von Krebsarten. Die teils schweren Nebenwirkungen, eingeschränktes Wirkungsspektrum und die intrinsische oder erworbene Resistenz zahlreicher Krebsarten gegenüber platinhältigen Verbindungen sind jedoch gravierende Nachteile dieser Krebsmedikamente. Ruthenium(III)komplexe haben sich aufgrund neuartiger Wirkungsmechanismen, höherer Selektivität und einem vergrößerten Anwendungsbereich als vielversprechende Kandidaten zur Entwicklung neuer Krebsmedikamente hervorgetan. Die First-In-Class Ruthenium(III)verbindung NKP-1339 (IT-139) zeigte bereits vielversprechende Ergebnisse in klinischen Studien. Es wird angenommen, dass im hypoxischen Tumorgewebe eine Aktivierung durch Reduktion des Metallzentrums zu Ruthenium(II) stattfindet. Interaktion mit dem zytosolischen Protein GRP78, sowie oxidativer Stress durch die Redoxaktivität des Metallzentrums sind die angenommenen Hauptfaktoren für die Aktivität von NKP-1339. Das Potential von organometallischen Ruthenium(II)komplexen als antineoplastische Medikamente wurde intensiv untersucht, und einige spannende Verbindungen befinden sich derzeit in fortgerschrittenen präklinischen Untersuchugen. Ein verheißungsvoller Ansatz ist die Koordination von bioaktiven Molekülen an organometallische Arenfragmente, wodurch die entsprechenden Komplexe mit diversen zellulären Zielstrukturen interagieren können.

1,2,3-Triazole besitzen interessante medizinische Eigenschaften und sind ein wichtiger Bestandteil in zahlreihen potentiellen Arzneiwirkstoffen. Sie können leicht durch Kupfer(I) katalysierte Husigen 1,3-dipolare Zykloaddition (Click-Chemie) hergestell werden. 4-Phenyl substituierte Triazole können potenziell als *N,C* Chelate fungieren und eine Reihe von Metallionen koordinieren. Die biologische Aktivität der abgeleiteten organometallischen Arenkomplexe und deren Eignung als Krebstherapeutika ist jedoch nahezu unerforscht. Im Zuge dieser Masterarbeit wurden sechs Phenyltriazole mit unterschiedlicher Substitution in Position 1 durch Kupfer(I) katalysierte Aklin-Azid Zykloaddition synthetisiert. Die Koordination der Triazole an organometallische Ruthenium(II) Arenfragmente lieferte die entsprechenden *N,C*-koordinierten Komplexe mit Chlorido Abgangsgruppe. Die Liganden und Komplexe wurden mittels 1D und 2D NMR Spektroskopie, HR-MS, Elementaranalyse, Schmelzpunkt, Löslichkeitsexperimenten und Kristallstukturanalyse charakterisiert. Zusätzlich wurde das Verhalten der Komplexe in wässriger Lösung und Reaktivität mit Biomolekülen durch ESI-MS Methoden untersucht.

ABBREVIATIONS

Å	Ångström, 10^{-10} m
$CDCl_3$	deuterated chloroform
CNS	central nervous system
CuAAC	copper-catalyzed azide-alkyne cycloaddition
cym	*p*-cymene
cys	L-cysteine
δ	chemical shift (NMR)
d	days
d	doublet, doubletic (NMR)
DCM	dichloromethane
DFT	density functional theory
DMSO-d_6	deuterated dimethyl sulfoxide
DNA	deoxyribonucleic acid
e.g.	*exempli gratia* (for example)
GRP78	78 kDa glucose-regulated protein
eq	equivalents
ESI	electrospray ionization
E. coli	*Escherichia coli*
et al.	*et alii* (and others)
EtOH	ethanol
g	gram
G	guanine (nucleobase)
GC	gas chromatography
h	hour
his	L-histidine
HIV	human immunodeficiency virus
HMBC	heteronuclear multiple bond correlation (NMR)
HSQC	heteronuclear single quantum coherence (NMR)
HR-MS	high resolution mass spectrometry
Hz	hertz (s^{-1})
Im	imidazole
Ind	indazole
J	coupling constant (NMR)

K	Kelvin
M	molar (mol L^{-1})
M	molecular ion (mass spectrometry)
MeOH	methanol
min	minute
met	L-methionine
MRI	magnetic resonance imaging
m/z	mass-to-charge ratio
NHC	N-heterocyclic carbene
NMR	nuclear magnetic resonance
PBS	phosphate buffered saline
pH	*pondus hydrogenii*
pK_a	log K_a (acid dissociation constant)
q	quadruplet (NMR)
ppm	parts per million
RAPTA	ruthenium(II) arene PTA
R_f	retention factor
s	singlet (NMR)
t	triplet, tripletic (NMR)
TGF-β	transforming endothelial growth factor
TLC	thin layer chromatography
TM	trademark
tzNHC	1,2,3-triazolylidene N-heterocyclic carbene
UV/VIS	ultraviolet / visible
VEGF	vascular endothelial growth factor
WHO	World Health Organization
1D / 2D NMR	one- / two-dimensional NMR spectroscopy
°	degree
°C	degree centigrade

TABLE OF CONTENTS

.

1. INTRODUCTION

1.1. General considerations

Cancer is one of the most feared diseases of the modern world. The global burden of cancer has more than doubled over the past 30 years. In 2008, over 12 million new cases of cancer were diagnosed and 7 million deaths could be attributed to cancer. Owing to growth and ageing of the world's population, a substantial rise in cancer incidences is expected over the next decades[1].

Malignant neoplasms were the second leading cause of death in Austria in 2013 with 28%, only surpassed by cardiovascular diseases with 38% (see **Figure 1**)[2].

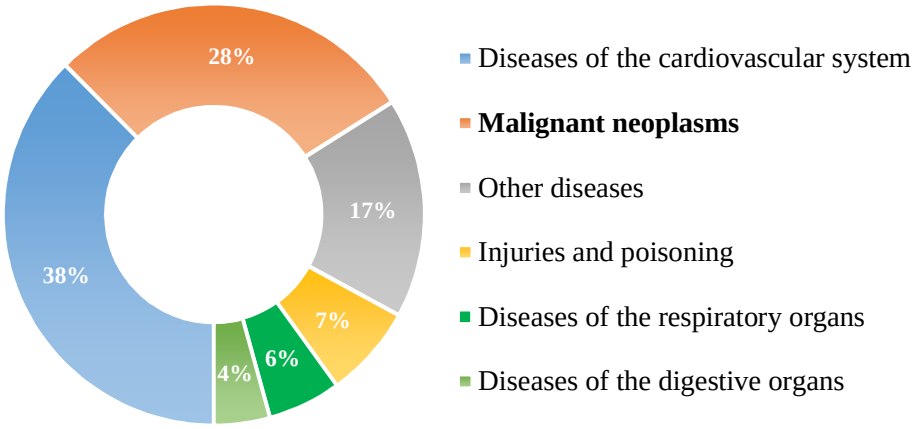

Figure 1: Causes of death in Austria in 2013

There are over 200 different types of cancer[3]. For Austrian men, malignant neoplasms of the prostate and testes (27%), colorectal cancer (27%), and respiratory cancer (16%) are responsible for most cancer incidences (2008)[4]. Among women, breast cancer (27%), colorectal cancer (23%), and cancer of the respiratory organs (13%) are predominant.

In less-developed countries, the percentage of cancerous diseases in the overall number of death is seemingly low. This can be explained by the comparatively higher incidence of infectious diseases and injuries. With the progress of medical care and control over infectious diseases, those countries are expected to see a considerable increase of cancer occurrences over the next decade[5], emphasizing that the development of novel anticancer agents is an issue of global importance.

1.2. Carcinogenesis

Cancer describes not just a single but many different diseases. Disorders in the cell cycle cause cell proliferation in an excessive and unregulated way. The formation of cancer, called carcinogenesis, is triggered by abnormal changes to the genetic material and can be induced by a variety of external and endogenous factors. Exposure to chemical mutagens (diet, smoking), viral infections (Epstein-Barr virus, human papillomavirus), bacteria (Helicobacter pylori), or high energy radiation are the most common exogenous causes for the development of cancer[6].

The broadest classification of cancer types relies on the type of organ from which the abnormal cell originates. However, a histological classification is preferable, because it gives a clearer indication of the future behavior and development of the growth. Carcinomas are derived from epithelial cells that line the skin or internal organs (lung, breast, prostate, colorectal cancer) and make up about 90% of all cancer indications. Tumors of the hematopoietic (blood-forming) and lymphoid tissues comprise leukemia, lymphoma and myeloma, while sarcomas stem from the mesenchymal cells of connective or supportive tissue (cartilage, fat, muscle), and central nervous system specific cancer types originate in the brain or CNS (glioma, blastoma). Although this system covers most prominent cancer occurrences, a considerable number of rare cancer subtypes elude classification according to these criteria.

The development of cancer is a multi-step process, which leads to the uncontrolled division of abnormal cells formed from healthy cells, and invasion into healthy tissue. First, carcinogens or hereditary factors cause mutations in the genetic material of in a single cell, a process called **initiation**. The damaged cell can either be repaired by tumor suppression proteins or undergo apoptosis, effectively neutralizing the danger posed by the mutation. If the initiated cell makes it through these safeguards, it may now undergo clonal growth and multiply rapidly. This **promotion** phase can be accelerated by endogenous or exogenous promoters and carcinogens. Down-regulation or inactivation of tumor suppression genes and up-regulation of oncogenes that aid tumor growth are constantly required, because the process is completely reversible up to this point. In the final stage called tumor **progression**, formerly benign tumor cells turn malignant, invade the surrounding tissue, and spread from the primary tumor throughout the body.

Most cancer cells are distinguished by several functional capabilities acquired during their development, the most prominent of which are listed below (see **Figure 2**).

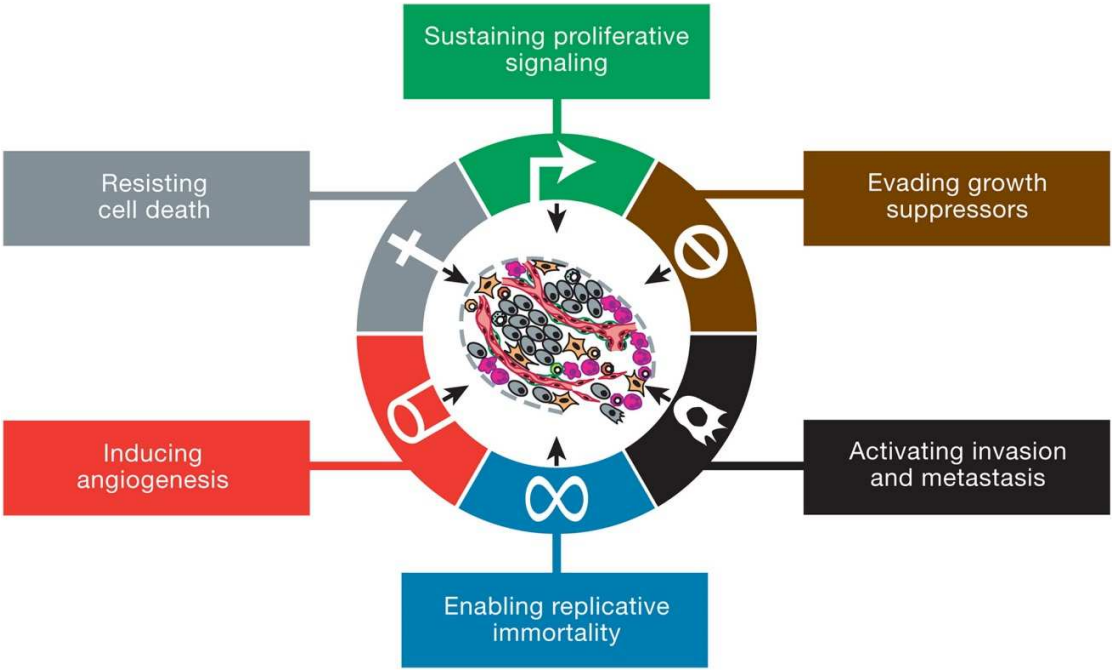

Figure 2: Selected functional capabilities acquired by cancer cells[7]

A normal cell divides and grows depending on external signals given off from surrounding cells. External growth factors activate a signal cascade, which eventually induces transcriptions of proteins and enzymes necessary for cell division. Cancer cells differ from healthy cells in that they can grow independent of external signal factors. The **sustained proliferative signaling** is achieved through inherent production of growth factors[8], overexpression of growth factor receptors or expression of constantly active receptors[9]. In contrast, several hormones (e.g. transforming growth factor TGF-β) act as tumor suppressors by counteracting the effect of growth factors. In order to ensure undisturbed unregulated cell division, cancerous cells need to develop **resistance to growth suppressors**[10].

Healthy cells have a last resort regulatory system in place that protects them from developing into abnormal or defect cells. A range of enzymes (e.g. caspase proteases) are constantly looking for disruptions in the cell cycle, absence of growth factors, DNA damage, or extrinsic death activator proteins. In case of activation, they induce cell death (apoptosis). **Resistance to cell death** may be acquired by cancer cells through mutation of the genes coding for apoptosis-regulating enzymes and receptors[11].

Cancer cells have the ability to replicate indefinitely, as opposed to healthy cells that undergo apoptosis after 50 to 60 cell divisions. The number of possible DNA replication cycles is determined by structures called telomeres, polynucleotide regions at the 3' end of chromosomes. After each cell replication, the telomeric DNA is shortened, up to the point where the telomeres can no longer ensure DNA stability and cell death is initiated. Cancer cells **develop immortality** by expressing an enzyme called telomerase, which elongates the telomeres with hexanucleotide fragments to maintain their length to circumvent cellular senescence[12].

Due to rapid uncontrolled growth, malignant neoplasms have a constant high demand for molecular building blocks, carbohydrates, and growth factors, and need to get rid of waste products to continue their expansion. The distance of malignant cells to the native blood supply increases with tumor size, effectively reducing their access to nutrients. As countermeasure, tumors release growth factors that stimulate the formation of new blood vessels to the tumor tissue (e.g. vascular endothelial growth factor VEGF, fibroblast growth factor FGF-2). This process called **angiogenesis** is also upregulated in healthy cells to treat vascular injuries, during exercise, and forms most of the cardiovascular system during embryonic development[13].

Malignant tumor cells have the ability to break away from the primary tumor and spread through the blood supply to form remote secondary tumors. Usually, cells are anchored to the extracellular matrix through adhesion proteins. If a healthy cell's adhesion proteins do not match the extracellular structures, apoptosis is triggered. On the other hand, cancer cells are expressed either with mutated or without anchoring proteins, enabling them to enter the blood stream, lymphatic system or body cavities without undergoing cell death[14]. Consequently, they may set themselves up in any part of the body and form **metastases**.

In contrast to malignant neoplasms, benign tumors lack the ability to invade healthy tissue or to metastasize. They resemble normal cells more closely than undifferentiated malignant cancer cells, and pose a lesser risk than malign growths due to their slower growth rate and inability to spread throughout the body. Nevertheless, benign tumors have the potential to develop into malignant cancers through a process called tumor progression[15], or exert negative health effects due to physical compression of neighboring tissues.

1.3. Cancer treatment

An extensive and growing arsenal of treatment strategies is needed to fight the diverse forms cancer can take on. The location and type of the tumor, progression of the disease and health of the patient are key factors for the selection of cancer treatment options. A treatment plan typically contains a combination of therapeutic strategies in order to optimize the outcome.

First, cancerous growths can be removed by **surgery**. Only localized and non-metastasizing tumors are potential candidates for surgical removal. Other treatments may be employed prior to surgery in order to shrink the tumor size (neoadjuvant), or to dispose of micrometastases and tumor remains after surgery (adjuvant). Additionally, surgical procedures and other cancer therapies can be used to control and diminish symptoms, while not aiming to cure the cancer (palliative).

Radiation therapy utilizes ionizing radiation to control or remove malignant cells. Radiation damages the genetic material of irradiated cells to induce apoptosis. In external beam radiation therapy, an external source of radiation emits radiation towards the tumor, which passes through healthy tissue to access the cancerous growth. Common side effects include severe nausea, damage to gonads causing infertility, inflammation of soft tissue and epithelial surface damage at the entrance points of the rays into the body. In order to minimize side effects in healthy cells, the ionizing radiation is sent into the body from various emitters placed around the patient. The emitted high energy radiation beams intersect at the target tissue, and healthy tissue is subjected to a far lesser dose. In contrast, internal radiotherapy (brachytherapy) relies on the insertion of therapeutic radionuclides in close proximity to the cancerous tissue, thereby decreasing the exposure of healthy cells to harmful radiation.

Chemotherapy, along with hormonal therapy and targeted therapy, makes up the class of pharmacotherapy for cancer. Chemotherapy employs a variety of natural, synthetic, or semi-synthetic small molecule pharmaceuticals to impair cell division and function by interaction with different cellular targets. Those targets usually are present in both healthy and cancerous cells. The rapid growth of cancer cells leads to a high demand in nutrients and molecular building blocks, therefore chemotherapeutic drugs are also accumulated. Nevertheless, fast-dividing healthy cells are equally affected, e.g. in the bone marrow, digestive tract, or hair follicles. Consequently, most side effects from therapy are caused by the poor selectivity, such as anemia, immunosuppression, gastrointestinal irritation, nausea and hair loss.

Hormone therapy employs drugs acting as hormone receptor antagonists in cancer cells, cutting off fast-replicating cells from their hormone supply. **Targeted therapy** relies on substances that specifically interfere with molecules solely involved in cancer growth or survival, like inhibiting angiogenesis or promoting cancer cell apoptosis[16]. In contrast, traditional chemotherapeutic agents affect targets present in all fast-dividing cells.

1.4. Classes of chemotherapeutic drugs

Chemotherapy agents can be divided into several major groups[17] depending on the mechanism by which they inhibit cell proliferation.

Alkylating agents are electrophilic compounds that can react with nucleophilic groups present in the nucleic acid bases of DNA. They disrupt replication and transcription of DNA through the formation of covalent bonds to nucleic acids. Poor selectivity and a range of side effects are caused by reaction with nucleophilic groups of other biomolecules (proteins, amino acids, etc.)

Antimetabolites disrupt DNA function by inhibiting the enzymes involved in DNA or nucleotide synthesis. Antimetabolitic agents are analogues of naturally occurring purine or pyrimidine bases, and therefore can be used as substrates by enzymes responsible for DNA synthesis[18]. Subsequently, they may either inhibit enzyme function (e.g. thymidylate synthase by 5-fluorouracil[19]), or lead to chain termination after being incorporated into DNA (e. g. gemcitabine, cytarabine).

Topoisomerase inhibitors also interrupt DNA replication. Prior to replication, the DNA strand has to be unwound, which is performed by the enzymes topoisomerase I and II. Topoisomerase inhibiting agents may stabilize the complex formed from DNA and topoisomerase I (e.g. camptothecines[20]) or topoisomerase II (e.g. anthracyclines[21]) to prevent further unwinding of the DNA chain.

Protein kinase inhibitors impair the cell signaling pathway by affecting protein kinase activity. These agents may interact with different cellular targets, such as the epidermal growth factor receptor EGFR (e.g. getifinib), the Abelson tyrosin kinase (e.g. imatinib), or multiple tyrosine kinases (e.g. the multi-targeting compounds sorafenib and sunitinib).

Mitotic inhibitors like the vinca-alkaloids (Vincristine, Vinblatine) or taxanes (Paclitaxel) affect the functionality of structural proteins (microtubuli) needed during cell division.

1.5. Metals in medicine

Inorganic metals play important roles in many critical processes in humans. Four main group metals (Na, Mg, K, Ca) are essential bulk elements, and at least ten transition metals (Fe, Cu, Zn, Se etc.) are currently considered essential trace elements. They are important for structure functions like skeletal support, cell wall integrity, stabilization of protein structures (Ca, Mn, Zn), as charge carriers for signal transduction, ion pump activity and muscle contraction (Na, K, Ca) and enzyme function and catalysis (Zn, Mg). Scarcity of those metals can lead to anemia symptoms and diseases. On the other hand, excess quantities of an essential metal can be as harmful as an insufficient supply. Additionally, nonessential metals taken up as environmental pollutants, especially heavy metals, can cause considerable adverse health effects.

Use of metals as medicinal agents goes back as far as ancient history. Ancient Egyptian texts describe the use of a copper derived mixture as sterilization agent for drinking water (2400 B.C.), or an early remedy for headaches (1500 B.C.). Therapeutic arsenic formulations were commonly employed in folk therapies for leukemia for centuries[22]. In modern times, research into bioinorganic medicinal chemistry has primarily been driven forward by the discovery of cisplatin and its chemotherapeutic potency in the 1960's. Nowadays, there is a range of metal-based **anticancer agents** in clinical use, some of which will be discussed further on. Antiproliferative drugs on metal basis are highly tunable through variation of metal and ligands to optimize target interaction, activity and targeting properties.

Metal compounds have found applications as **MRI contrast agents**, mainly complexes of unpaired electron rich Gd(III), Mn(II) and Fe(III) ions[23]. MRI relies on the difference in ^{1}H NMR resonances due to varying water content between tissues. Contrast agents shorten the relaxation time of water molecules in neighboring tissue[24], thus facilitating the evaluation of MRI spectra. Several gadolinium containing complexes have been approved for clinical use (e.g. Magnevist™, Gadvist™), and are the most commonly used MRI contrast agents.

Another common field of application is metal-derived **radiopharmaceuticals**. Radioactive tracer atoms are employed either as ionic salts or complexes in medical imaging, and therapeutic radionuclides find use as radiation sources in brachytherapy (see section 1.3).

Additionally, metal and metal derived compounds are utilized as antiarthritic agents, antiinfective medicines, antihypertensive drugs[25], insulin mimetics[26], and antiulcer agents.

1.5.1. Platinum-based anticancer agents

The antineoplastic properties of cisplatin were serendipitously discovered in 1965 by Rosenberg *et al.*[27] during investigations on the effect of electrical currents on *E. coli* growth.
Owing to the experimental setup and fortunate external circumstances, several platinum complex species were formed by redox reactions on the platinum electrodes, which completely halted bacterial cell division. It was shown that cisplatin was primarily responsible for the antiproliferative effect[28]. Cisplatin was approved for clinical use in 1978 mainly on the basis of work by Einhorn *et al.* [29] and has been successfully employed for the treatment of testicular and ovarian cancer, bladder, cervical, and small cell lung cancer[30]. Unfortunately, cisplatin therapeutic regimens entail a variety of side effects, such as nephrotoxicity (dose-limiting), peripheral neuropathy, tinnitus, hearing loss, and severe nausea. Some tumor types acquire resistance to cisplatin after the first treatment cycles, or are inherently resistant. Side-effects can be ameliorated by administering anti-emetics, adequate hydration and diuresis.

Driven by the success of cisplatin, several platinum(II) compounds have been developed and undergone clinical evaluation. Replacement of the chlorido leaving groups with cyclobutanodicarboxylato ligand afforded carboplatin. This cytostatic agent exhibits diminished side effects but retained activity compared to cisplatin, therefore enabling a high-dose chemotherapeutic regimen. Investigations on ammine group variation revealed a promising class of compounds containing 1,2-diammino-cyclohexane ligands as a stable chelating moieties, culminating in the discovery of oxaliplatin[31]. In contrast to cisplatin, oxaliplatin shows a significantly altered activity profile and therefore activity in many cell lines with intrinsic cisplatin resistance (e.g. colorectal cancer). Leaving group variation has been shown to influence the toxicity profile, while activity modulation is achieved by substitution of ammine ligands due to change in the structure of the resulting DNA adducts.

Cisplatin, carboplatin and oxaliplatin are the only platinum(II)-based antineoplastics that are in worldwide clinical use and are shown below (see **Figure 3**).

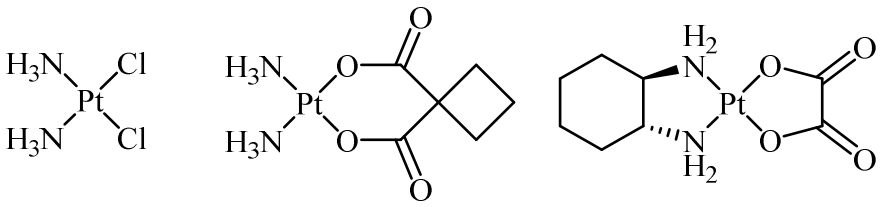

Figure 3: Planar platinum(II) complexes cisplatin (left), carboplatin (middle) and oxaliplatin (right)

Cisplatin is administered intravenously, after which it spreads in the body through the blood stream and rapidly diffuses into tissues. Subsequent undesired binding of cisplatin to sulfur-rich plasma proteins is one of the main mechanisms of inactivation and approximately 90% of the administered drug is bound to abundant and cysteine-rich albumin[30]. Cisplatin may enter cells by passive diffusion, mediated by copper transporter proteins[32] or other unidentified active transport mechanisms. There is a significant decrease of chloride concentration from the extracellular (100 mM) lumen to the cell nucleus (2-30 mM), which facilitates cisplatin activation. One or both chlorido leaving groups are replaced by water molecules forming a charged complex. The aquated cisplatin complex exhibits high reactivity towards nucleophilic DNA bases, especially N7 of guanine, but also N7 of adenine. First, a monofunctional cisplatin-DNA adduct is formed, which usually reacts further to bifunctional inter-strand (< 5%), intra-strand, or protein-DNA crosslink products. Up to 60-65% of adducts are intra-stand crosslink products of two neighboring guanine nucleobases (1,2-d(GG), see **Figure 4**). This pseudo-alkylation bends the DNA by 30-40 ° towards the major groove of the double helix and unwinds it by approx. 13 °, therefore preventing recognition of the DNA by enzymes necessary for cell replication and transcription. If the platinated DNA is not repaired by the cellular repair machinery, apoptosis is induced.

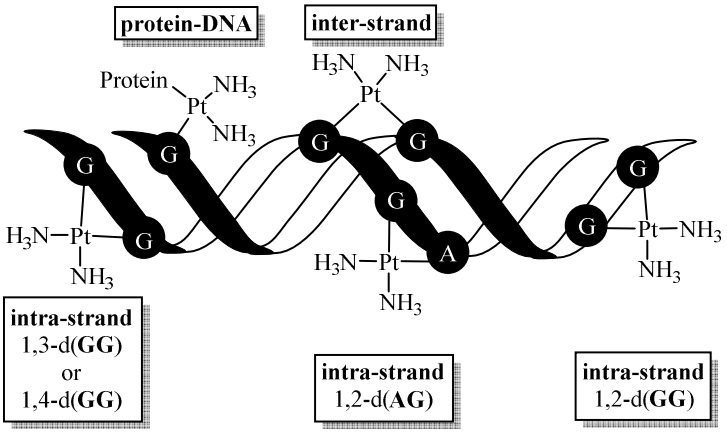

Figure 4: Different crosslink products formed by cisplatin

To improve the pharmacological properties, diminish side-effects and overcome resistance problems, research has focused on the development of novel platinum drugs. Various octahedral platinum(IV) complexes show exciting prospects for clinical applications. They are thought to undergo activation by reduction to platinum(II) in the cancer cells. Exciting future prospects currently under investigation are *trans*-platinum(II) complexes as cytostatics, monofunctional platinum(II) complexes, multinuclear platinum(II) compounds, and many more.

1.5.2. Ruthenium anticancer agents

The narrow spectrum of efficacy and deplorable side effects of platinum-based drugs has stimulated research on the development of non-platinum antineoplastic compounds with a broader spectrum of activity, higher selectivity and novel modes of action.

Ruthenium complexes exhibit various characteristics that make them preferable over or good substitutes for platinum compounds. Under physiological conditions, ruthenium is able to adapt oxidations states II, III, and perhaps IV, and readily interchanges between them due to low energetic barriers. The exchange of the leaving group is essential for interactions with biological targets and is influenced by the chloride concentration, pH value and the coordination sphere of the complex[33]. The preferred octahedral coordination geometry gives ample room for possible modification and interaction with biomolecules other than DNA. Furthermore, ruthenium is suspected to bind to transferrin due to similarity to iron. Transferrin is an iron transport protein, to which ruthenium may either bind instead of iron, or more likely bind to a different place of the carrier. Cancer cells are distinguished by high nutrient (iron) requirements and consequently show increased expression of transferrin receptors[34].

NAMI-A, an octahedral ruthenium(III) complex with a DMSO and imidazole ligand in axial position and four equatorial chlorido groups (see **Figure 5**): [ImH][*trans*-$RuCl_4$(DMSO)(Im)] (Im = imidazole, DMSO = dimethylsulfoxide) exhibits very low *in vitro*[35], yet high activity *in vivo* and high selectivity for solid metastasizing tumors. The antimetastatic effect is the most distinguishing feature of NAMI-A and is cause for synergistic effects in combination therapy with cisplatin or classic organic cytostatic drugs. Some of the many postulated mechanisms for the antimetastatic activity of NAMI-A are rearrangement of the cytoskeleton, disruption of the actin-dependent adhesion of metastases and clearance of metastasizing cells from primary tumor tissue.

In contrast, the first-in-class ruthenium(III) complex NKP-1339 (IT-139) developed by the Keppler group[36] shows significant activity both *in vivo* and *in vitro*, especially against colorectal cancer lines. The complex features two axial indazole ligands and four equatorial chlorides: (InH)[*trans*-$RuCl_4(In)_2$] (In = indazole), see **Figure 5**. The major advantage of NKP-1339 is the superior aqueous solubility compared to its predecessor KP1019, therefore clinical investigations were continued with NKP-1339[37].

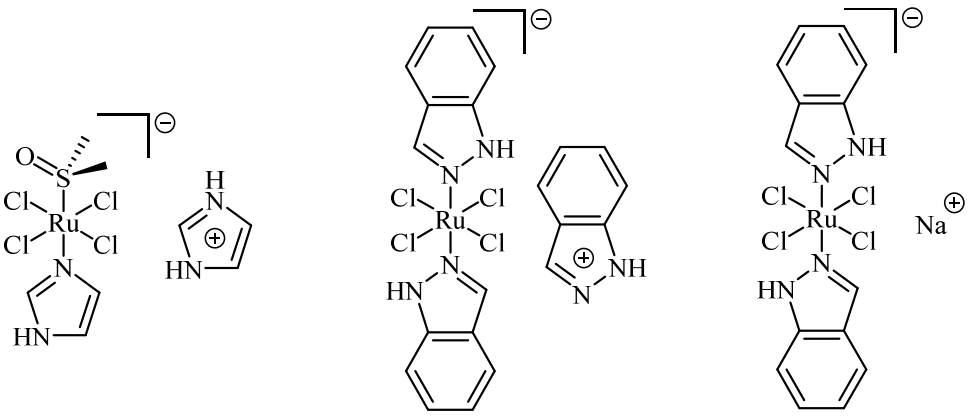

Figure 5: NAMI-A (left), KP1019 (middle), NKP-1339 (right)

The high activity of NKP-1339 is supposed to be derived from the reduction of the metal center under the hypoxic conditions of the tumor tissue (activation by reduction). Due to the rapid proliferation of cancer cells, the tumor tissue is deprived of oxygen and nutrients, and therefore has to rely on glycolysis for energy production. Metabolites from glycolysis decrease the pH value and together with rapid growth induced hypoxia provide an ideal reductive environment for the reduction of ruthenium(III) to ruthenium(II)[38]. Labilization of the Ru-Cl bond comes along with the changed oxidation state and facilitates the electrophilic binding to biomolecules. The selective accumulation of ruthenium compounds in the cells due to their iron mimicking properties and interaction with blood proteins such as albumin and transferrin, along with the activation in the cancer tissue may account for the significantly decreased systemic toxicity of ruthenium(III) compounds. Recent investigations have revealed that direct interactions with DNA are not the primary cause for the antiproliferative effect of NKP-1339. In contrast, the cytosolic protein GRP78, a key factor of the unfolded protein response (UPR), has been suggested to be a main target of this drug. In addition, the redox-active metal center is able to generate ROS, which provides oxidative stress and induces apoptosis *via* the mitochondrial pathway. However, further detailed investigations on the mode of action are currently performed.

The success of the first-in-class drug NKP1339 has stimulated the development of ruthenium-based metallodrugs. Especially Ru(II)-arene complexes of the form [(η^6-arene)Ru(X)(Y)(Z)] (X,Y,Z = donor atoms of mono- or polydentate ligands) have shown promising results and several representatives are in an advanced preclinical stage. These organometallics are characterized by a different mode of action compared to clinically applied metal-based drugs. Anticancer activity, selectivity, pharmacological properties, biomolecule interaction, and cell accumulation can be easily fine-tuned comparatively by variation of the ligand sphere.

Pioneering work has been done by the groups of Sadler and Dyson, which has resulted in the promising drug candidates RM175 and RAPTA-C (see **Figure 6**).

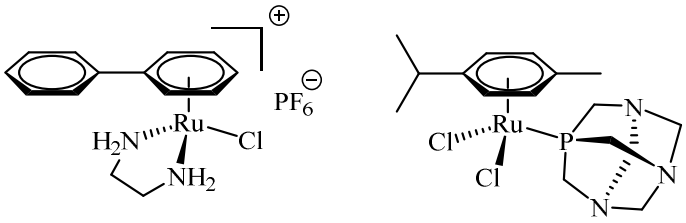

Figure 6: RM175 (left), RAPTA-C (right)

In reference to their structural similarity to a piano stool (the polyhapto arene ligand acts as the seat and the three remaining coordination sites as legs), these half-sandwich compounds are known as “piano-stool”-complexes.

Sadler and coworkers have extensively studied ruthenium(II) arene complexes of the form [(η^6-arene)Ru(chel)X], featuring an either neutral or anionic bidentate chelating ligand and a halide leaving group, resulting in charged or neutral complexes. Leaving group variation revealed that chlorido substituted complexes showed highest activities in combination with a bidentate ethylendiamine ligand. One of the lead compounds, RM175 is currently in preclinical evaluation and demonstrates *in vitro* cytotoxicity similar or greater than carboplatin *in vivo*[39]. RAPTA complexes developed by Dyson and coworkers are one of the few cytotoxic ruthenium arene compounds featuring three monodentate ligands. One coordination site is occupied by the characteristic pta ligand (1,3,5-triaza-7-phosphoadamantane), while two potential chlorido leaving groups are also present. Generally, complexes featuring three monodentate ligands do not show significant activity, presumably to rapid ligand hydrolysis. In contrast, **r**uthenium **a**rene **pta** complexes (RAPTA) show moderate cytotoxicity *in vitro* but remarkably high selectivity for cancer cells over healthy cells. *In vivo*, antimetastatic effects similar to NAMI-A and in some cases reduced growth of the primary tumor were observed[40].

Leaving group variation can impact the cytotoxic potency by modification of the ligand exchange rate and thus the generation of the highly reactive aqua-species. Variation of the arene ligand has also been shown to be of importance in cases (e.g. RAPTA and Sadler-type compounds[41]). The non-leaving chelating ligand has the greatest influence on the properties of the resulting complex. Depending on the coordination moiety of the ligand (e.g. *O,O*-, *N,N*-, *S,O*-chelates etc.), different stabilities under physiological conditions are achieved.

1.6. Triazoles as pharmacophores

The discovery of the copper-catalyzed azide-alkyne cycloaddition (CuAAC) for the regioselective synthesis of 1,4-disubstituted-1,2,3-triazoles (see **Figure 7**) independently by Sharpless[42] and Meldal[43] in 2002 has led to a phenomenal rise in triazole-related research. The reaction stands out due to mild reaction conditions, high yield, facile workup, wide scope and insensitivity to functional groups. Consequently, the CuAAC reaction fulfills the demanding criteria set by Barry Sharpless to earn click-chemistry status[44]. Due to the unparalleled selectivity, reliability, and scope of this conversion, it is oftentimes simply referred to as "Click reaction".

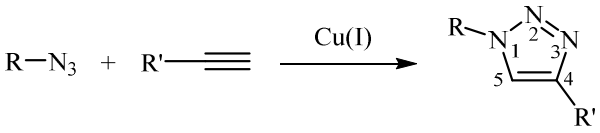

Figure 7: Copper(I)-catalyzed azide-alkyne cycloaddition

Historically, 1,2,3-triazoles were prepared by thermal Huisgen 1,3-dipolar cycloaddition of azides with alkynes. Unfortunately, the neat reaction of an azide 1,3-dipole and an dipolarophile alkyne shows poor regioselectivity and tends to afford mixtures of the 1,4- and 1,5-regioisomers.

Incorporating 1,2,3-triazole motifs into candidate drugs is attractive because of their high stability to metabolic degradation and hydrogen bonding capabilities to facilitate interaction with biological targets[45]. 1,2,3-Triazoles have attracted attention as peptide bond isosteres, due to the similar steric arrangement and electronic properties to peptide bonds without adverse effect on the biological activity[46]. A variety of medicinal agents contain triazoles as an integral part of their structure, including HIV-1 reverse transcriptase inhibitors[47], antituberculosis[48], antifungal and antibacterial agents[45].

Moreover, a multitude of potential anticancer drug candidates containing triazole functions have been reported. Herein, 1,2,3-triazoles are oftentimes used for the synthesis of analogues of compounds with known antiproliferative activity (e.g. resveratrol[49], α-GalCer[50] and many more) or as linking group. Other triazole anticancer agents under investigation with related structure to the compounds discussed in this thesis are e.g. 4-aryl triazole based angiogenesis inhibitors[51] and 1,4-disubstituted 1,2,3-triazole antiproliferative compounds[52] (see **Figure 8**).

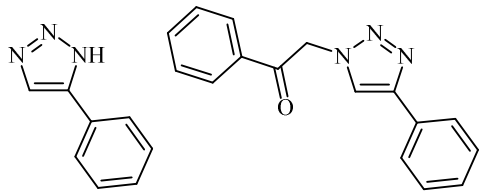

Figure 8: Triazole compounds under preclinical investigation

1.7. C-H activation *via* ruthenium(II) catalysis

In recent years, there has been extensive research by the Ackerman group on the functionalization of aromatic C-H bonds by conversion with alkenes in the presence of a ruthenium(II)-arene catalyst[53]. Recently, the ruthenium-catalyzed direct arylations of arenes with triazol-1-yl substituents as directing groups to achieve regioselectivity was reported[54,55] (see **Figure 9**).

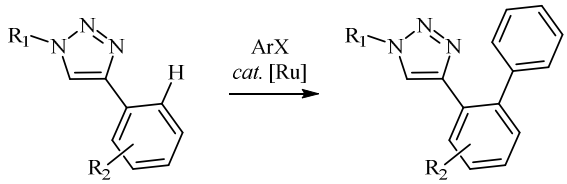

Figure 9: Ruthenium(II)-catalyzed direct arylation

Mechanistic investigations[56,57] have suggested that C-H bond metalation to form a ruthenium(II) arene complex with *N,C*-coordinated ligand is a key step in the catalytic cycle. In related investigations, Liang *et al.* [58] isolated an *N,C*-coordinated ruthenium(II) arene complex of 2-phenyl-pyridine by reaction of the ligand with stoichiometric amounts of $[Ru(p\text{-cym})Cl)]_2$ and an acetate base (e.g. sodium acetate). Due to electronic and steric similarity of 2-phenyl-pyridine to 4-phenyl-substituted triazoles, it was suspected that triazoles could coordinate in a similar way (see **Figure 10**).

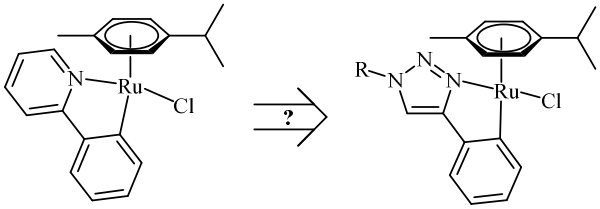

Figure 10: *N,C*-coordinating 2-phenyl-pyridine complex synthesized by Liang *et al.* (left), *N,C*-coordinating triazole complex to be explored (right)

Excited by this hypothesis, we were intrigued to explore the potential of triazole based *N,C*-coordinated ruthenium complexes as anticancer agents.

1.8. Triazole complexes as anticancer agents

Despite their prevalence in chemical catalysis[59], compounds featuring a ruthenium-carbon bond have been largely neglected as anticancer agents. Alongside the established classes of ruthenium(II)–arene anticancer agents (see section 1.5.2), *N*-heterocyclic carbenes (NHC's) have experienced increasing popularity as ligand system for the development of bioactive compounds. Silver-, gold-, platinum- and palladium-NHC complexes have received considerable attention[60,61]. Additionally, ruthenium-NHC's were observed to show promising enzyme inhibition and cytostatic effects[62].

In 2008, Albrecht and coworkers[63] pioneered the synthesis of transition metal complexes bearing 1,3,4-substituted 1,2,3-triazolylidene NHC's (tzNHC's). The first systematic investigations on the biological activity of ruthenium(II) and osmium(II) arene complexes featuring tzNHC's was performed by the Dyson group[64]. The synthesized complexes were observed to undergo rapid hydrolysis in aqueous solution leading to immediate activation, and a number of them show antiproliferative activity in the low micromolar range. Furthermore, they exhibit noteworthy selectivity for cancer call lines over non-tumorgenic cell lines, up to 200-fold (see **Figure 11**). The accessible modifiability and strong metal-ligand carbene bond[65] encourage the use of this ligand system in the biological environment.

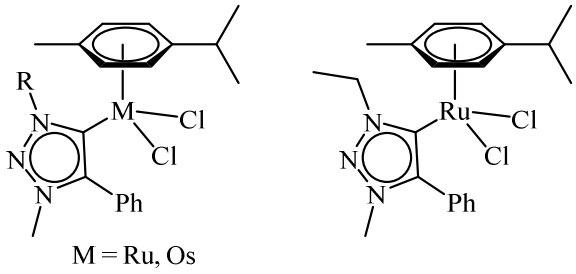

Figure 11: General structure of M(II) arene tzNHC complexes (left), highly cancer cell line selective Ru(II) arene tzNH complex (right)

To the best of our knowledge, *N,C*-coordinated ruthenium arene triazole complexes have not been investigated for their biological activity and anticancer potential up to now.

2. RESULTS AND DISCUSSION

The goal of this thesis was the synthesis of novel *N,C*-coordinated piano-stool Ru(II)(*p*-cymene) complexes (see **Figure 12**) based on 1,4-disubstituted 1,2,3-triazole ligands. The influence of different functional groups in position 1 of the triazole ring on the properties of the corresponding complexes was to be explored. Ligands and complexes were characterized *via* ^{1}H, ^{13}C and two-dimensional NMR techniques, X-ray diffraction analysis, high-resolution mass spectrometry, and elemental analyses. Additionally, melting points, solubilities, investigations on the behavior in aqueous solution and interaction with amino acids by ESI-MS were performed.

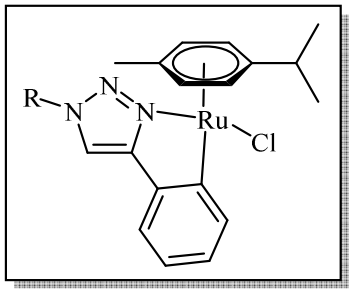

Figure 12: General structure of the synthesized complexes

2.1. Synthesis of the ligands

In order to regioselectively synthesize 1,4-disubstituted 1,2,3-triazole ligands, the copper-catalyzed azide-alkyne cycloaddition was employed.

The proposed catalytic cycle for the CuAAC reaction (see **Figure 13**) is largely based on DFT calculations and kinetic measurements. First, interaction of the copper(I) catalyst and the alkyne affords an intermediary π-alkyne-copper(I) species. Copper coordination induces a significant pH decrease (approximately 9.8 pH units[66]), which enables deprotonation even in neutral aqueous environments to form the σ-alkynyl-copper(I) compound **II** (step A). Subsequently, the azide attacks the alkyne-bearing copper as a nucleophile (step B). The copper(I)-acetylide experiences further activation through π-coordination of another copper(I) center[67] (not pictured). The reduced alkyne electron density enables cyclization to afford a copper(III) vinylidene metallacycle (step C). Transannular association of the *N*1 lone pair with the C5 copper π* orbital allows ring contraction of the metallacycle[68] (step D). Subsequent protonation regenerates the catalyst and regioselectively affords the 1,4-disubstituted 1,2,3-triazole **VI** (step E).

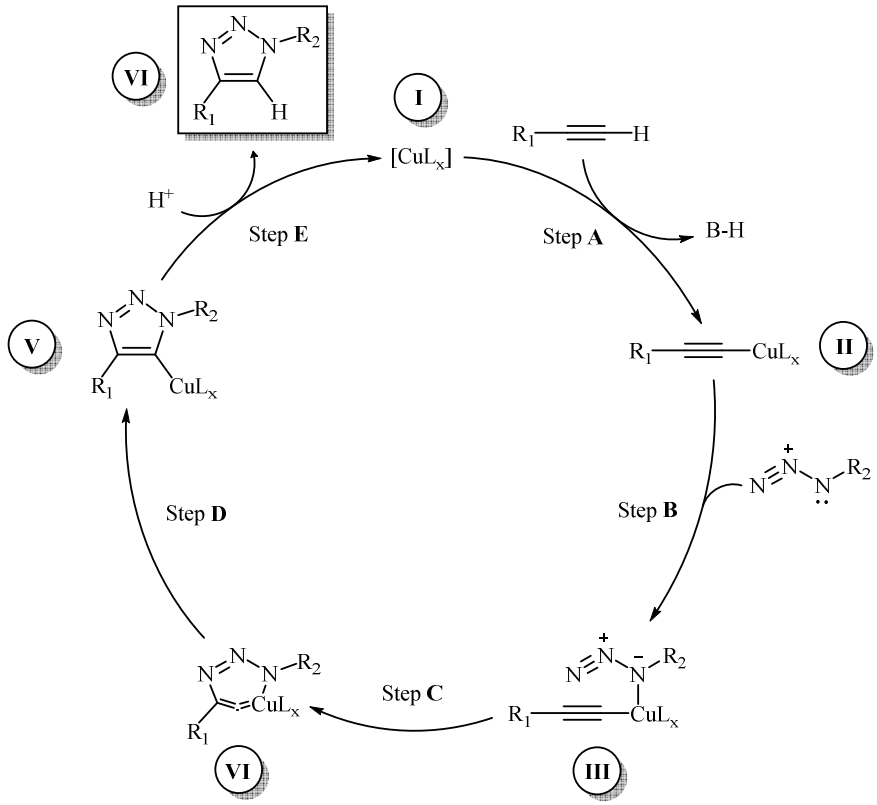

Figure 13: Proposed catalytic cycle for CuAAC[66]

It was decided to synthesize a total number of six triazole ligands **1a–f** in order to cover a broad range of functional groups, while still maintaining a degree of variation within a series. Compounds **1a,b** feature a benzylic residue, **1c,d** an aliphatic residue, and **1e,f** ester derivatives (see **Figure 14**).

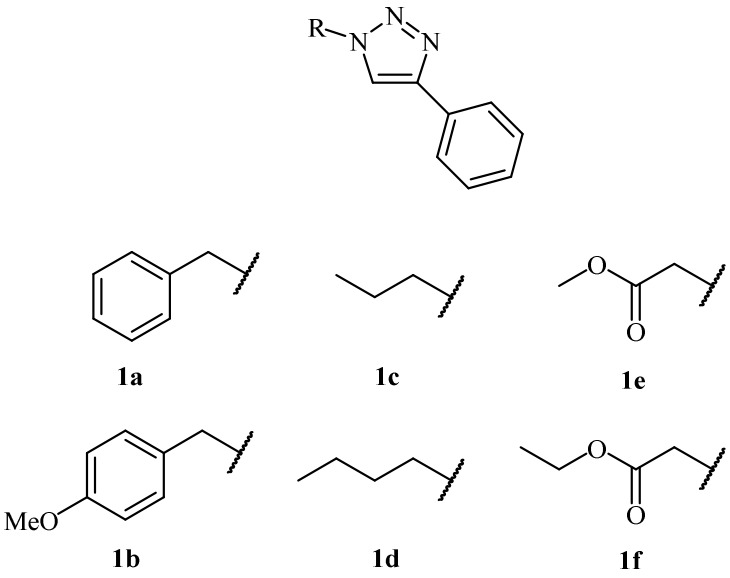

Figure 14: Desired triazole ligands **1a–f**

In order to synthesize the desired 1,2,3-triazole ligands, a facile and robust method for the generation of organic azides for the CuAAC reaction had to be found. Initial test reactions were performed according to the method developed by Alvarez *et al.*[69]by reacting benzyl bromide with a 1.1-fold excess of sodium azide in DMSO and stirring at room temperature. After a short reaction time of 1.5 h, the reaction mixture was quenched with water and the azide product extracted into diethyl ether. Evaporation of the solvent *in vacuo* afforded the desired azide in excellent yields (> 90%). Subsequently, benzyl azide was reacted with phenyl acetylene in DMSO / water (1:1) in the presence of copper(I), generated *in situ* from copper(II) sulfate and sodium ascorbate (0.2 eq each). The product was precipitated with water, filtered off and purified on silica to give the desired 1-benzyl-4-phenyl 1,2,3-triazole **1a**.

Unfortunately, this synthetic procedure is not suitable for the synthesis of the whole series **1a–f**. Short chained organic azides pose the danger of explosive decomposition when isolated, which increases with lower molecular weights. As per a commonly employed empirical rule of thumb, at least six carbons per azide group in a molecule have to be present to sufficiently decrease its reactivity and render it bench stable[70].

Benzyl azide and derivatives could be isolated and stored at room temperature, but shorter alkyl derivatives were deemed too dangerous to be isolated. Hence, the previously stated reaction conditions could not be applied.

In 2005, Kacprzak[71] reported a one-pot strategy for the synthesis of 1,2,3-triazole from corresponding organic halides, featuring in situ generation of azides from halide precursors and subsequent copper(I) catalyzed cycloaddition of an alkyne, therefore avoiding the isolation of short chained azides. A large excess of sodium azide would lead to the competitive formation of *NH*-triazole, by reaction of alkyne with the remaining inorganic azide. In this procedure, the azides were generated *in situ* from halide precursors by reaction with an equimolar amount of sodium azide in DMSO, which necessitated a prolonged reaction time for the azidation step. After 12 to 24 h, water, sodium ascorbate, copper(II) sulfate and alkyne were added and stirred at room temperature. Precipitation of the product was completed by addition of water, simple filtration and purification on silica afforded a variety of 1,2,3-triazoles in high yield and purity. Using this one-pot procedure (see **Figure 15**), the triazole ligands **1a–f** were synthesized in moderate to excellent yields (34 – 93%), with alkyl derivatives **1c,d** giving the lowest yields. Overall, the yield decreased with lower molecular weight of the corresponding alkyl azide.

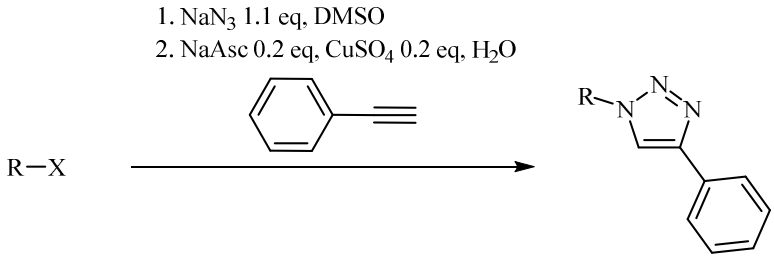

Figure 15: General reaction scheme for the synthesis of 1,2,3-triazole ligands **1a-f**

No significant formation of the *NH*-triazole was observed, irrespective of whether 1.0 or 1.1 equivalents of sodium azide were used. In favor of a shorter reaction time, 1.1 eq of azide were employed for subsequent reactions. Monitoring the rate of conversion by TLC proved to be difficult, as the azides either showed practically the same retention factor (R_f) as the precursor halides, and alkyl derivatives did not absorb in the UV/VIS range. In the literature, GC analysis is routinely employed to check the progress of the reaction. However, the reaction time for the azidation step was varied between 2 hours and as much as 5 days and the conversion was monitored by ^{1}H NMR. Full conversion was detected after 24 hours of reaction time for alkyl derivatives, while benzyl azides were quantitatively formed after 2 h.

2.2. Synthesis of the respective organometallic complexes

Utilizing reaction conditions similar to those published by Liang *et al*., the triazole ligands **1a–f** were reacted with 1 eq of the precursor ruthenium dimer bis[dichlorido(η^6-*p*-cymene) ruthenium(II)] in the presence of 1.1 equivalents of sodium acetate as base in anhydrous methanol (see **Figure 16**). After only a few moments of reaction time, the free metal dimer was quantitatively converted to a carboxylate intermediate, as confirmed by ^{1}H NMR. Reaction of the triazole ligands with sodium methoxide as deprotonating agent and ruthenium precursor in methanol showed no conversion, which is evidence that the carboxylate activated [Ru(*p*-cymene)] complex is required for the *N*,*C*-coordination of 1,2,3-triazoles to ruthenium(II)-arene fragments.

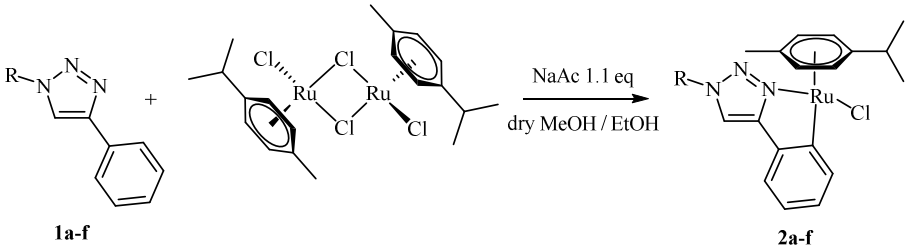

Figure 16: General reaction scheme for the synthesis of Ru(II) piano-stool complexes **2a–f**

As the reaction progresses, the product precipitates as microcrystalline yellow solid. It was observed that a concentrated solution of triazole and dimer is needed to drive the conversion towards the complex product (approximately 1 mL methanol per 40 mg dimer). Under these conditions, the alkyl triazoles **1c–f** are completely dissolved, while benzyl triazoles **1a,b** are suspended with only traces of the free triazole in solution. The conversion rate was monitored primarily by evaluating the phenyl protons in ^{1}H NMR, due to loss of symmetry and significant change in shift upon coordination (see section 2.4.1). Usual reaction times range between one day (alkyl derivatives), to 5 days (benzyl derivatives), after which a maximum conversion of around 80% was reached. Neither heating to reflux nor microwave irradiation at various temperatures between 40 to 120 °C accelerated the reaction or gave full conversion.

After the maximum conversion was reached, the product was collected by filtration and washed with small amounts of cold methanol to separate the remaining free triazole and the carboxylate activated Ru(II) precursor complex. The crude product was dissolved in dichloromethane and filtered in order to separate inorganic salts. Evaporation of the solvent *in vacuo* afforded the products in elemental analysis purity in average to good yields (40 – 71%).

2.3. Characterization of the ligands

2.3.1. ^{1}H NMR

The triazole scaffold proton is usually found as a sharp singlet in a range between 8.56 and 8.63 ppm. The protons corresponding to the phenyl ring in position 4 of the triazole scaffold are typically found at 7.31 to 7.84 ppm. Due to the symmetry of the aromatic ring, the five protons are observed as distinct, usually well-defined signals. Going from downfield to upfield signals, protons H7/11 in *ortho* positon form a doublet, protons H8/10 a doubletic doublet, and H9 a doubletic doublet as well. As the coupling constant between the germinal aromatic protons are similar in size, the doubletic doublet signals superimpose to give pseudo-triplets. Substitution of the triazoles in position 1 shows very little effect on both phenyl and triazole proton shifts. As to be expected, the shift of the singlet corresponding to the methylene bridge in position 5 depends greatly on the substitution on the side chain, ranging from 5.55–5.65 (benzyl derivatives **1a–b**), 4.36–4.39 (alkyl derivatives **1c–d**) to 5.45–5.48 (ester derivatives **1e–f**). The electron withdrawing effect of the triazole ring can be seen especially well in ^{1}H NMR spectra of the alkyl derivatives. Methylene groups close to the triazole ring (H12) are significantly shifted downfield, while CH_2 groups near the terminal methyl group of the alkyl chain (H15) are far less exposed to the deshielding effect of the triazole ring.

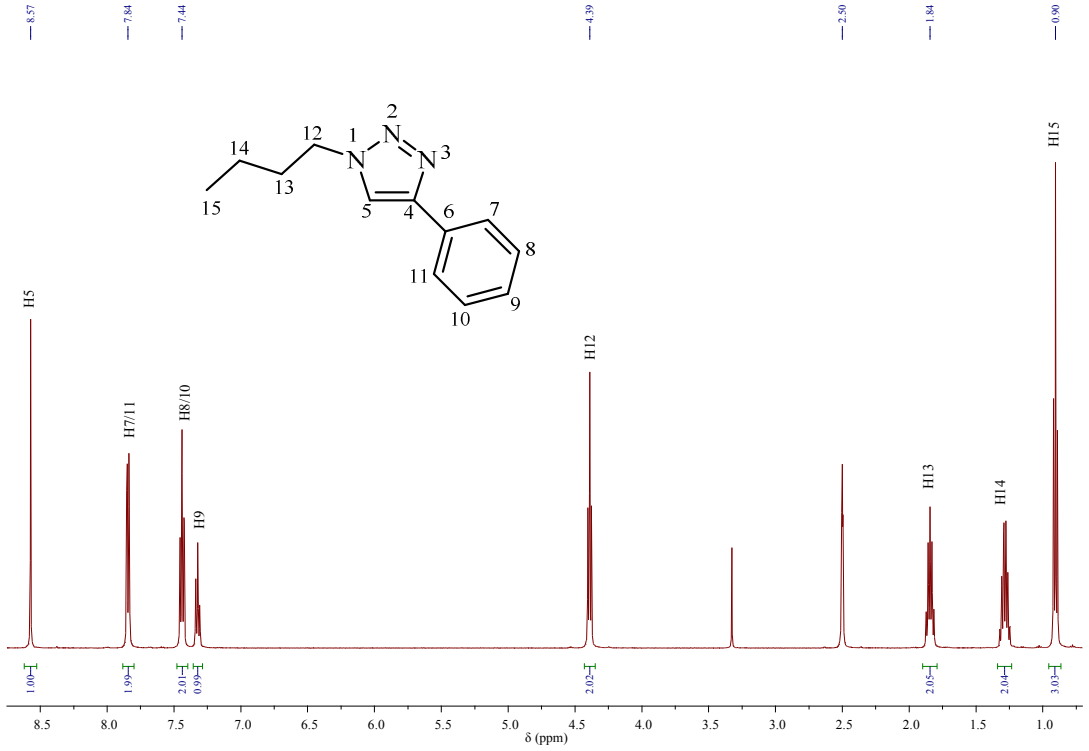

Figure 17: ^{1}H NMR spectrum of ligand **1d**

2.3.2. ^{13}C NMR

The quaternary carbons of the phenyl ring and triazole ring are found downfield from the aromatic CH signals, as to be expected. Due to the unhindered rotation along the C4-C6 bond, only 4 signals for the phenyl ring can be observed. Similar to the ^{1}H spectrum, side chain substitution in position 1 again has very little influence on the chemical shifts of the triazole scaffold and phenyl ring carbons.

.

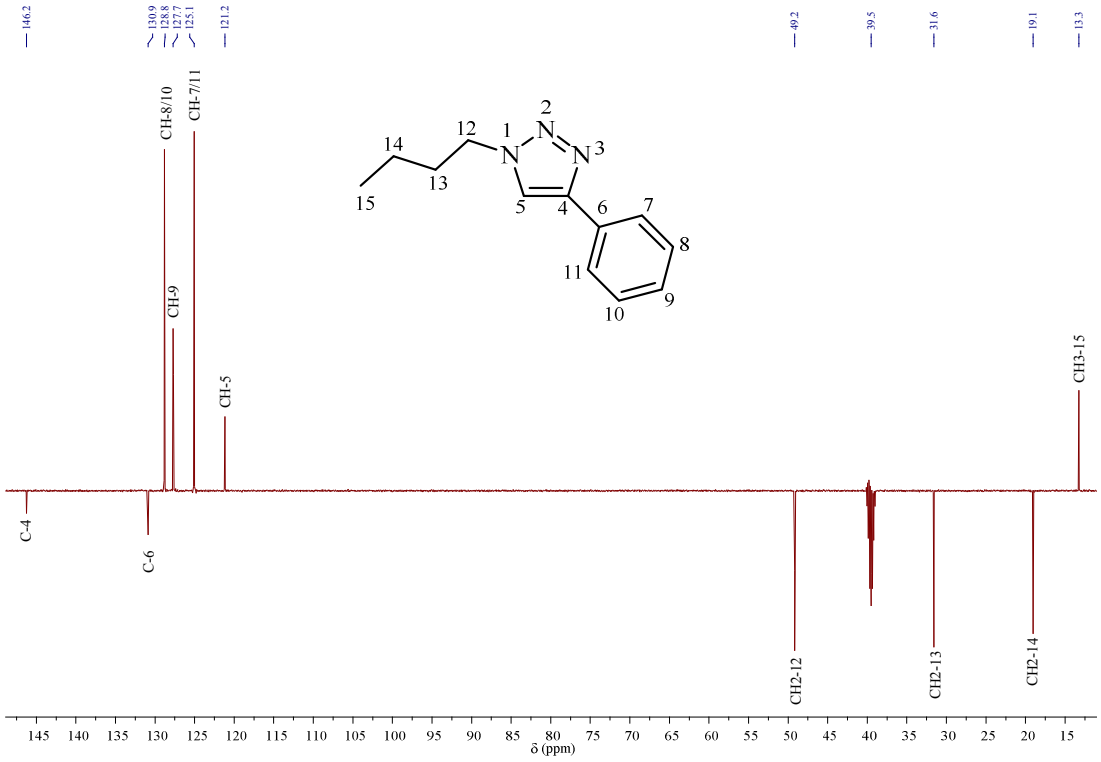

Figure 18: ^{13}C NMR spectrum of ligand **1d**

2.3.3. HR-MS

High resolution mass spectrometry with electrospray ionization and a quadrupole time-of-flight detector was also employed to verify the formation of the synthesized compounds. The samples were dissolved in a mixture of methanol and water, and dispersed into an aerosol by exposure to high voltage. Compared to other ionization methods like inductively coupled plasma (ICP) ion sources or electron ionization (EI), ESI gives a low degree of fragmentation and therefore is known as a soft ionization method.

As a result, only quasi-molecular ions by addition of a proton $[M+H]^+$ or sodium cation $[M+Na]^+$ (see **Table 1**) to the otherwise uncharged triazole ligands were observed. In ligand spectra, the signal with highest intensity consistently corresponded to the sodium adduct $[M+Na]^+$, followed by the proton adduct $[M+H]^+$ and a dimeric species with added sodium cation $[M+M+Na]^+$ (see **Figure 19**).

Table 1: Found and calculated m/z values of compounds **1a–f**

Ligand ion $[M+Na]^+$	**m/z**	
	found	calculated
1a	258.1003	258.1002
1b	288.1102	288.1107
1c	210.1002	210.1002
1d	224.1158	224.1158
1e	240.0747	240.0743
1f	254.0896	254.0900

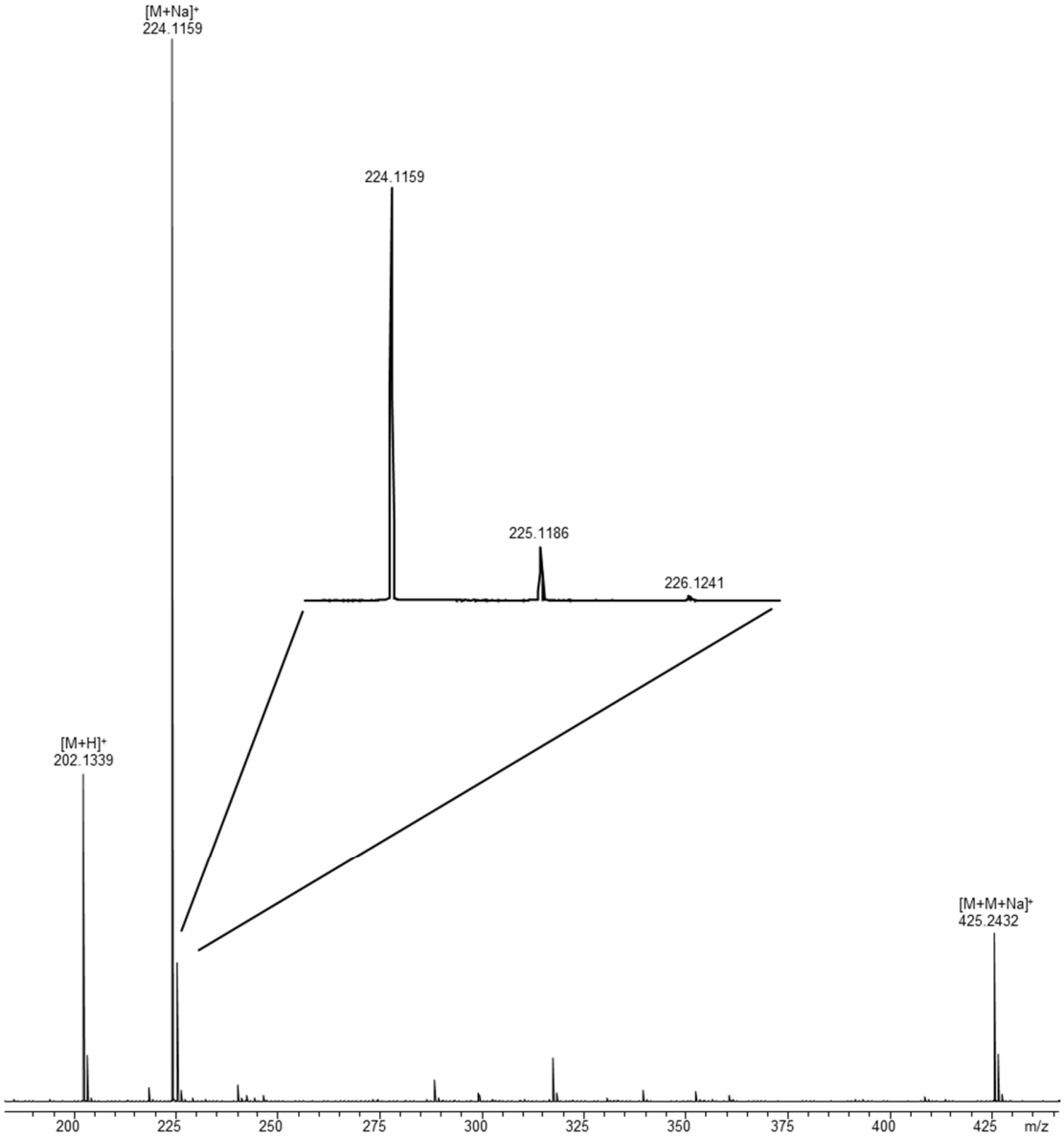

Figure 19: High resolution mass spectrum of ligand **1d**, with enlarged $[M+Na]^+$ peak showing the isotopic distribution pattern

2.4. Characterization of the complexes

2.4.1. ^{1}H NMR

The most prominent effect of coordination on the ligand signals is the break of symmetry in the phenyl ring, resulting in four distinct phenyl signals, two doublets (H8, H11) and two pseudo-triplets (H9, H10). It was expected that the subtraction of electron density from the phenyl ring due to coordination would cause a downfield shift of all phenyl signals. However, only the proton in *ortho* position to the coordinated carbon is shifted downfield, by approximately 0.7 ppm, while the other aromatic protons are displaced to lower chemical shifts. A possible explanation for this behavior could be π-backbonding of electrons from the metal d-orbitals to a π* antibonding ligand orbital.

Due to the introduction of the coordinated metal atom as a chiral center, the diastereotopic methylene bridge protons in position 12 couple with each other (^{2}J-coupling), which was not observed for the free ligand. Similar effects were reported for related ruthenium(II) arene compounds[72]. Besides that, the side chain protons are not influenced by the coordination and are found in a similar range as for the non-coordinated triazoles.

The protons of the η^{6}-coordinated *p*-cymene ligand are found in the typical range for Ru(II)(*p*-cym) complexes. The aromatic signals are observed between 5.15 – 5.55 ppm as well-defined doublets and can be attributed unambiguously to the respective aromatic protons ($Hc_{1,2}$, $Hd_{1,2}$) by 2D NMR techniques and evaluation of the roof effect. Interestingly, one C-proton is significantly shifted lowfield compared to the other aromatic protons.

In complexes **2a,b** with benzyl triazole ligands, the aromatic cymene protons that couple with each other (c_1 with d_1, c_2 with d_2) are located next to each other in the spectrum (c_1-d_1-d_2-c_2 going from upfield to lowfield). In alkyl triazole complexes **2c–f** however, the d-protons switch places (c_1-d_2-d_1-c_2, see **Figure 20**). As variation of the side chain in position 4 has very little influence on the electronic properties of the *N,C*-coordination motif, additional interaction of the side chain with either the metal center or the arene ligand is suspected to be the reason for this phenomenon.

The isopropyl group of the arene signal is observed as two non-equivalent methyl signals due to inhibited inversion caused by coordination of the sterically demanding ligand. They are found as doubletic signals by coupling with the proton in position f, which in turn is split into a septet.

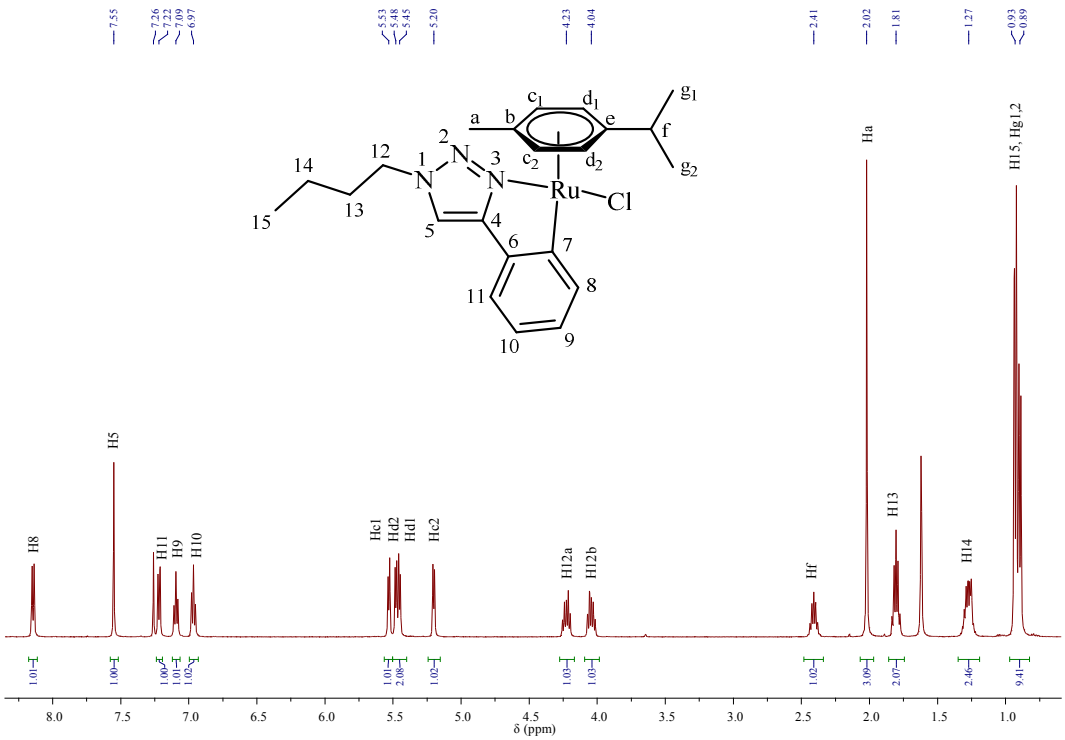

Figure 20: ^{1}H NMR spectrum of complex **2d**

2.4.2. ^{13}C NMR

Similar effects of coordination as observed in the ^{1}H spectra are found in the corresponding ^{13}C NMR experiments (see **Figure 21**). The symmetry of the phenyl ring is broken, which is why six distinct phenyl signals are found. The signal corresponding to the carbon bonded to ruthenium (C-7) is shifted the farthest downfield (around 176 pm), followed by the quaternary carbon in position 6 (around 135 ppm). Concerning the remaining phenyl protons, the farther they are located away from the coordinating carbon, the lower their chemical shift becomes. Analogously to the ^{1}H spectrum, the aromatic carbons in *meta* and *para* position to the coordination site are found at a higher chemical shift than in the free ligand.

When comparing the different complexes, the aromatic carbon atoms of the *p*-cymene ligand (CH-c and CH-d) are found in the same sequence (CH-c_1, CH-d_2, CH-c_2, CH-d_1) regardless of the coordinated triazole. In contrast, the sequence of the corresponding signals in ^{1}H NMR are different for benzyl and alkyl triazole derived complexes (see section 262.4.1.).

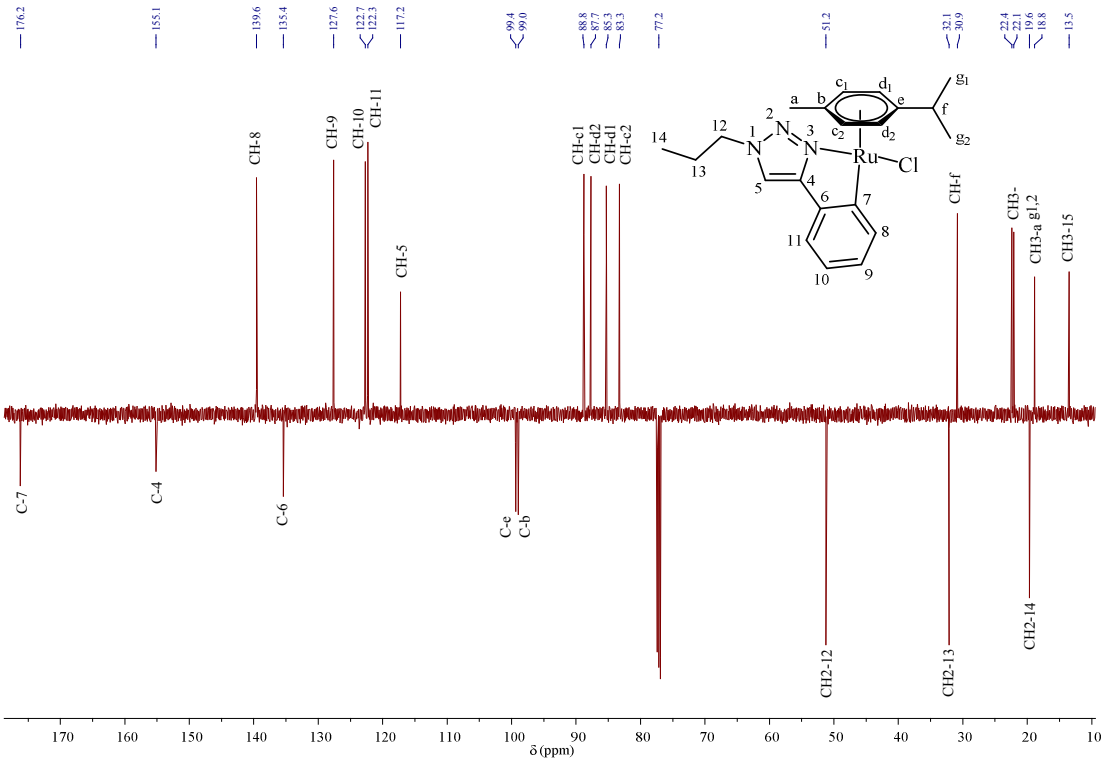

Figure 21: ^{13}C NMR spectrum of complex **2d**

2.4.3. HR-MS

Analogously to the ligands, their corresponding complexes **2a–f** were also analyzed by high resolution mass spectrometry with electrospray ionization and quadrupole time-of-flight detection.

The two characteristic peaks observed corresponded to the sodium cation adduct of the complex $[M+Na]^+$ and the single positively charged species $[M–Cl]^+$ (see **Table 2**), where the chlorido ligand was abstracted. Usually, the molecular ion with hydrolyzed chloride was found to be the peak with highest intensity (see **Figure 22**) except for the propyl derived complex **2c**, in which the characteristic $[M+Na]^+$ and $[M–Cl]^+$ peaks were approximately the same size, and the methoxy benzyl complex **2b**, in whose spectrum the sodium adduct $[M+Na]^+$ made up the main peak. These results suggest a high hydrolytic lability of the ruthenium-chlorido bond, which is cleaved to a considerable point even in the presence of 1% water.

The experimentally found isotope pattern of the peaks is in accordance with the calculated isotope distribution.

Table 2: Found and calculated m/z values of compounds **2a–f**

Complex ion $[M–Cl]^+$	**m/z**	
	found	calculated
2a	470.1184	470.1164
2b	500.1292	500.1270
2c	422.1176	422.1164
2d	436.1326	436.1321
2e	452.0914	452.0906
2f	466.1060	466.1063

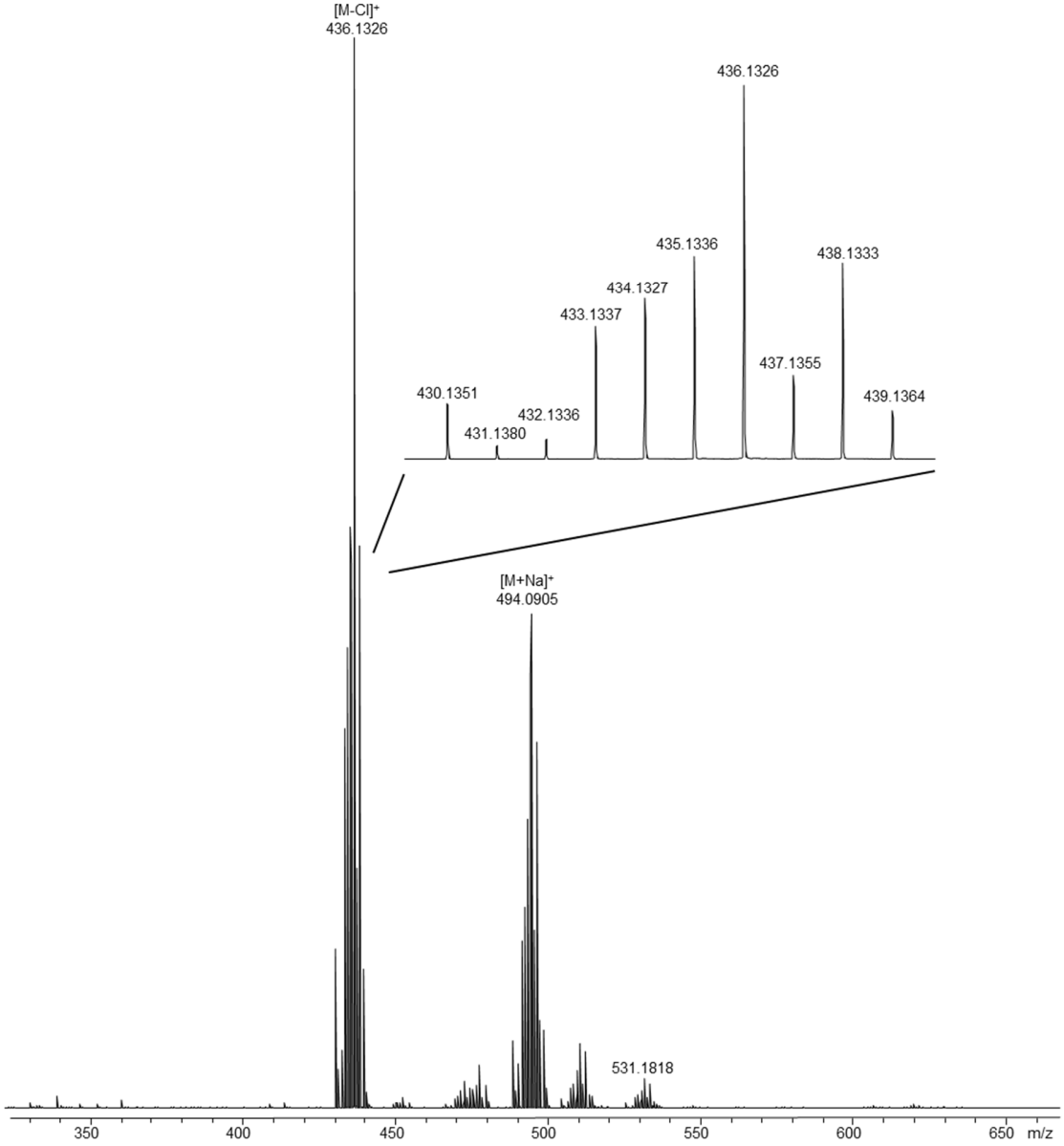

Figure 22: High resolution mass spectrum of complex **2d** with enlarged $[M+Na]^+$ peak showing the isotopic distribution pattern

2.4.4. X-ray diffraction analysis

Single crystals of **2d** and **2e** were obtained by slow diffusion from dichloromethane and hexane. Both structures crystallized in the "piano-stool" configuration, the typical half-sandwich coordination geometry. The complexes possess a pseudo-tetrahedral geometry at the ruthenium(II) atom, where the arene ligand occupies three coordinating sites, forming the "seat", and three other ligands represent the "legs".

Complex **2d** crystallizes in the tetragonal $I4_1/a$ space group, while **2e** is a representative of the triclinic $P\overline{1}$ space group. Both compounds crystallized without additional solvent molecules and exhibited a low degree of disorder, which renders the comparison of molecular parameters possible (see **Figure 23**).

The M–Cl distances are in the same range for both alkyl and ester derivative (see **Table 3**), which was expected due to the low influence of the side chains on the electronic properties of the coordination moiety. Generally, the side chain variation was not observed to have a significant influence on the coordination geometry.

A pronounced effect of coordination is the impact on the aromaticity of the phenyl ring. Carbon-carbon bonds in a non-substituted phenyl group are usually around 1.4 Å long[73]. The bond length to carbons in *ortho* position to the C7-Ru bond are slightly elongated (1.41 Å), which can be attributed to the electron withdrawing effect exerted by coordination. In contrast, the remaining aromatic carbon-carbon bonds are shortened. The bond length decreases with increasing distance to the coordinated carbon atom, and can be related to the increase in chemical shift observed in ^{1}H and ^{13}C NMR.

The bidentate triazole ligand and the metal center form an almost planar five membered ring, which can be seen from the respective torsions (e.g. C4-C6-C7-Ru: **2d** = 3.9 °, **2e** = 2.2 °). The theoretically planar geometry is distorted by steric interaction with the other bound ligands and the metal center.

Furthermore, the coordination locks the phenyl and triazole rings in a fixed conformation in respect to each other. As a consequence, the two rings are approximately located in the same plane, as can be seen from the negligible torsion around the phenyl-triazole bond (N3-C4-C6-C7: **2d** = 0.48 °, **2e** = 1.81 °).

Table 3: Bond lengths, angles and torsions of **2d** and **2e**

Compounds			2d	2e
Metal to ligand	**Ru - Cl**	**[Å]**	2.4301(4)	2.4161(3)
	Ru - N3	**[Å]**	2.0845(13)	2.0736(10)
	Ru - C7	**[Å]**	2.0740(15)	2.0694(12)
Triazole ring	**N1 - N2**	**[Å]**	1.3436(18)	1.3429(14)
	N2 - N3	**[Å]**	1.3241(18)	1.3170(14)
	N3 - C4	**[Å]**	1.3646(19)	1.3687(15)
	N1 - C5	**[Å]**	1.349(2)	1.3540(15)
Phenyl ring	**C4 - C5**	**[Å]**	1.370(2)	1.3776(16)
	C4 - C6	**[Å]**	1.454(2)	1.4545(16)
	C6 - C7	**[Å]**	1.414(2)	1.4169(16)
	C7 - C8	**[Å]**	1.401(2)	1.4022(16)
	C8 - C9	**[Å]**	1.394(2)	1.3983(17)
	C9 - C10	**[Å]**	1.388(3)	1.3924(18)
	C10 - C11	**[Å]**	1.387(2)	1.3939(17)
	C11 - C6	**[Å]**	1.394(2)	1.3985(16)
C6 – C7 - Ru		**[°]**	116.54	116.53
C4 – N3 - Ru		**[°]**	117.40	117.67
N3 – Ru - Cl		**[°]**	88.82	89.25
Cl – Ru – C7		**[°]**	85.98	85.89
C7 – Ru – N3		**[°]**	77.27	77.43
C4 – C6 – C7		**[°]**	113.58	113.50
C4 – C6 – C11		**[°]**	123.43	123.91
N3 – C4 – C6 – C7		**[°]**	0.48	1.81
C6 – C4 – N3 - Ru		**[°]**	3.17	5.03
C4 – C6 – C7 - Ru		**[°]**	3.92	2.17

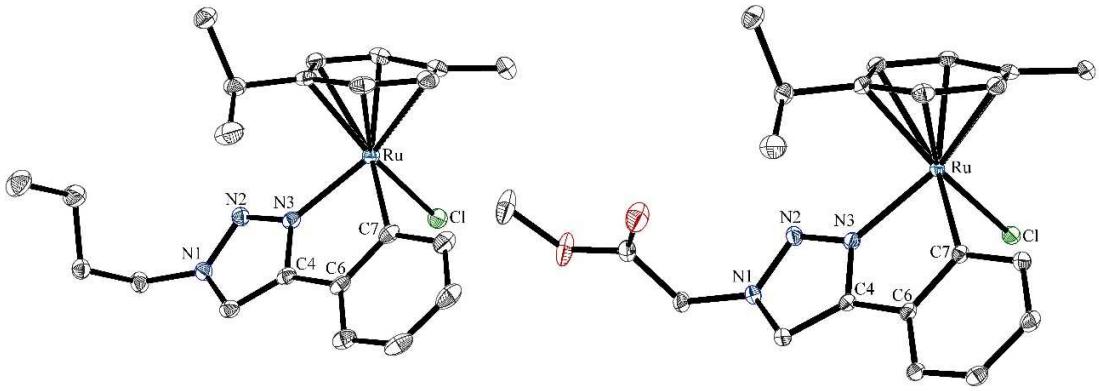

Figure 23: Crystal structures of **2d** and **2e**

The unit cells of the compounds contain the (*R*) and (*S*) enantiomers in a racemic mixture, suggesting that there is no preference towards any stereoisomer (see **Figure 24**). Additionally, it can be seen that the triazole ligands of the corresponding enantiomers are stacked on top of each other, which may be explained by π-stacking interaction of the aromatic rings. The two triazole rings are slightly offset, with a distance of 3.67 Å (**2e**) between the centers of mass. In literature[74], the typical interplanar distance for aromatic stacking interaction is around 3.3 to 3.8 Å. It is therefore reasonable to assume, that the complexes in the unit cell interact through π-stacking of the parallel displaced triazole rings.

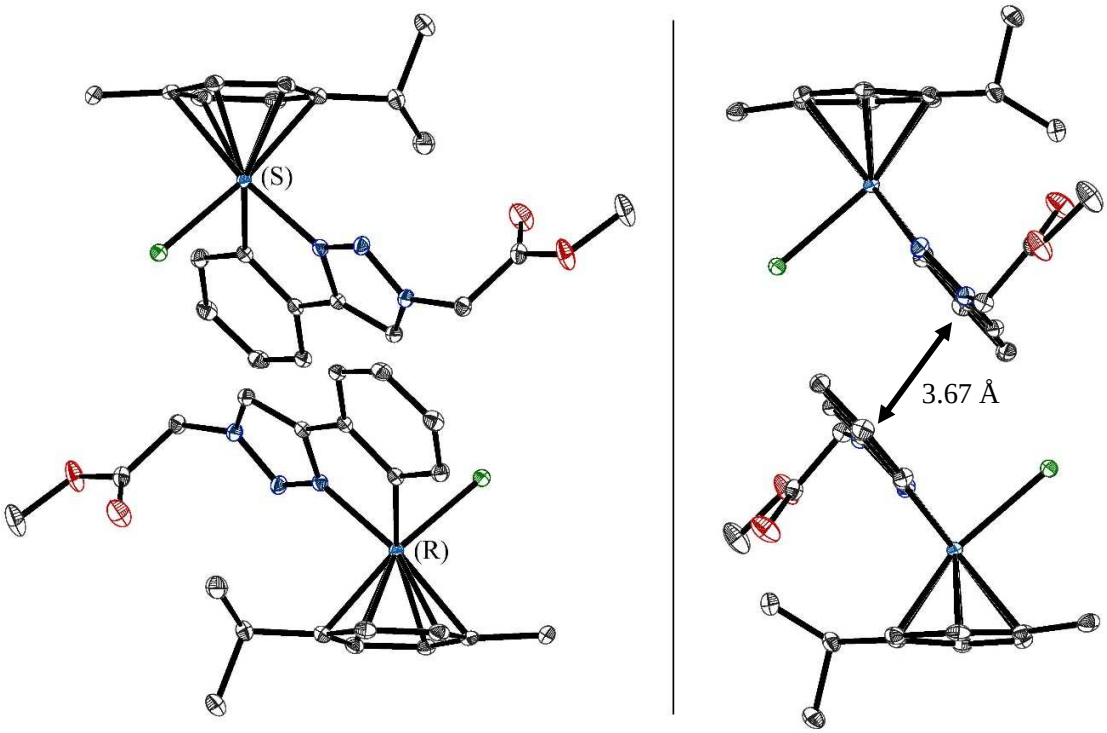

Figure 24: Front (left) and side (right) view of the primitive cell of **2e**

Table 4: Data collection and refinement parameters for **2d** and **2e**

Compound		**2d**	**2e**
Goodness of fit		1.090	1.062
Temperature	**[K]**	100	100
Crystal size	**[mm]**	0.228 x 0.236 x 0.269	0.215 x 0.249 x 0.322
Crystal system		tetragonal	triclinic
Space group		I 41/a	P-1
a	**[Å]**	28.6971(11)	9.8442(3)
b	**[Å]**	28.6971(11)	9.9364(3)
c	**[Å]**	10.0994(5)	11.6969(5)
α	**[°]**	90	71.6070(10)
β	**[°]**	90	72.9617(14)
γ	**[°]**	90	88.0034(10)
Volume	**[Å^3]**	8317.1(8)	1035.95(6)
Z		16	2
$\rho_{calc.}$	**[g/cm3]**	1.505	1.561
h range		-34 to 34	-13 to 13
k range		-34 to 34	-14 to -13
l range		-12 to 12	-16 to 16
No. reflections		147992	28312
No. parameters		248	257

2.4.5. Stability in aqueous medium

The stability of complexes **2a–f** in aqueous solution was investigated by ESI-MS measurements. The method (described in section 3.1.6.) relies on the incubation of a 50 µM solution of complex in 0.5% DMSO / water for a time of 48 h at 37 °C, during which samples were collected and analyzed via ESI-MS. Comparison of the peak areas of the respective peaks in the MS spectra allowed to draw conclusions on the ratio of the species present in aqueous solution over time. However, the peak area depends on the ionizability of the detected species, thus no quantitative, but rather qualitative information is obtained. Consequently, the following percentage values refer to the share in overall peak area and cannot be interpreted as definite molar ratios.

The two prominent compounds detected in the stability measurements were the complexes with chloride abstracted $[M\text{-}Cl]^+$ and the DMSO adduct of the aforementioned species $[M\text{-}Cl+DMSO]^+$. For HR-MS measurements, the complexes were dissolved in a mixture of acetonitrile and methanol with 1% water. Herein, not only the $[M\text{-}Cl]^+$ species but also an intact sodium adduct $[M+Na]^+$ were observed. The absence of the $[M+Na]^+$ peak in a 0.5% DMSO / water solvent system suggested that the complexes **2a-f** were quantitatively and rapidly hydrolyzed in aqueous medium.

In all complex solutions, the intensity of the DMSO adduct peak $[M\text{-}Cl+DMSO]^+$ approached a maximum of 64 to 68% compared to the characteristic peak $[M\text{-}Cl]^+$. The incubated solutions of **2b,c** and **2e,f** had already reached the maximum DMSO adduct concentration at the initial (0 h) measurement, and no changes were observed over 48 h of incubation time. For complexes **2a** and **2d**, a smaller initial $[M\text{-}Cl+DMSO]^+$ peak (27 – 34%) was found at the initial measurement. Nevertheless, these compounds also reached the maximum DMSO adduct content after one (**2c**) or three hours (**2a**) of incubation (see **Table 5**).

Table 5: Proportional peak area of $[M\text{-}Cl+DMSO]^+$ peak at the start of incubation and approached maximum DMSO adduct content after incubation

Compound	**2a**	**2b**	**2c**	**2d**	**2e**	**2f**
0 h	27	68	64	34	67	65
Maximum	68	68	64	66	68	66

Additionally, the hydrolysis of the ester functionality bearing complexes **2e,f** to the corresponding carboxylic acid was observed. After 48 h of incubation, two to three percent of the overall peak area corresponded to the free carboxylic acid (**2e:** $[M\text{-}CH_2\text{-}Cl+DMSO]^+$) or (**2f:** $[M\text{-}C_2H_4\text{-}Cl+DMSO]^+$). It has to be noted that this does not represent the absolute ratio of the compounds in solution. Most likely, only a small part of the hydrolysis product was observed. The main share of the carboxylic acid complex is deprotonated, therefore has an overall neutral charge and cannot be detected by MS.

2.4.6. Amino acid interaction in aqueous medium

In order to study the binding affinity of amino acids toward the metal complexes, compounds **2a-f** were incubated with L-cysteine, L-histidine, or L-methionine according to the previously described method. These amino acids were selected, because histidine, and mainly the sulfur-containing amino acids, are known for their reactivity toward ruthenium(II) arene complexes.

None of the complexes **2a-f** were observed to form any kind of amino acid adduct during the incubation time of 48 h. The only difference to the spectra collected during stability investigations (see section 352.4.5) was the increased rate of ester hydrolysis in the presence of histidine, leading to an increase of the carboxylate-DMSO adduct peak $[M\text{-}CH_2\text{-}Cl+DMSO]^+$ from 2–3% to 4–6%. This can be explained by the higher basicity of histidine compared to the other amino acids, which could increase the pH of the incubated solution thus favoring ester hydrolysis. The use of buffered solutions to confirm this hypothesis is subject for further research.

The pronounced unreactivity of the complexes to amino acids makes them interesting drug candidates, because interaction with proteins and amino acids is a main pathway for the excretion of metal based drugs from the body, and the source of diverse side effects.

3. EXPERIMENTAL PART

3.1. Equipment and Methods

3.1.1. NMR spectra

NMR spectra were recorded using a Bruker *FT-NMR spectrometer Avance III*^{TM} in deuterated dimethyl sulfoxide (DMSO-d_6) or deuterated chloroform ($CDCl_3$). 2D NMR spectra were measured in a gradient-enhanced mode.

3.1.2. Elemental analyses

Elemental analyses were carried out at the Microanalytical Laboratory of the University of Vienna, using a PerkinElmer *2400 Series II CHNS/O Elemental Analyzer* for CHN analyses, and a Eurovector *EA3000 Elemental Analyzer* for CHNS analyses.

3.1.3. Melting points

Melting points were determined with a Büchi *Melting Point M-560*.

3.1.4. X-ray structures

X-ray diffraction measurements were performed on a Bruker *D8 VENTURE* system equipped with a multilayer monochromator and a Mo K/a INCOATEC microfocus sealed tube (λ = 0.71073 Å) spectrometer at 100 K. Single crystals of **2d** and **2e** suitable for x-ray diffraction analysis were grown by slow diffusion from dichloromethane/*n*-hexane at 4 °C.

3.1.5. HR-MS

High resolution mass spectra were recorded in the Core Facility for Mass Spectrometry (Faculty of Chemistry, University of Vienna) on a Bruker *Maxis UHR qTOF Mass Spectrometer* by direct infusion. Data files were analyzed using Bruker data analysis software ESI Compass 1.3 and Data Analysis 4.0.

3.1.6. ESI-MS

Stock solutions of complexes in DMSO were prepared and diluted to concentration of 100 µM complex in 1% DMSO/ H_2O. For amino acid binding experiments, the complex solution was incubated with an equal volume of water or 100 µM aqueous amino acid solution (either L-cysteine, L-histidine, or L-methionine). Aliquots were taken after 0, 1, 3, 6, 24 and 48 hours of incubation at 37 °C and stored at -20 °C until analysis.

Electrospray ionization mass spectra were recorded on a Bruker *AmaZon SL ion trap* mass spectrometer by direct infusion. Data files were analyzed using Bruker data analysis software *Compass 1.3* and *Data Analysis 4.0*. Samples were diluted with water / methanol (1:1) to a concentration of 5 µM and injected with a flow rate of 240 µL/h. Following instrument settings were used: dry temperature: 180 °C, nebulizer: 8.00 psi, dry gas: 6.00 L/min, capillary voltage: - 4500 V, end plate offset: - 500 V, ICC target: 50000, maximum accumulation time: 200.0 ms, scan range m/z: 70 - 1200, target mass m/z: 600, average of 8 scans.

3.1.7. Solubility

The solubility was determined in phosphate buffered saline solution (pH 7.4) containing 1% DMSO. The compound was dissolved in DMSO and diluted with PBS to an overall concentration of 1% DMSO/PBS. The maximum solubility refers to the highest analyte concentration, at which no precipitation could be observed.

3.2. Materials

3.2.1. Solvents

All solvents were purchased from commercial sources and used without further purification. Methanol and ethanol for coordination reactions were distilled and stored over molecular sieve (3 Å) prior to use.

Methanol (HPLC grade, Fisher) and Millipore water (*Milli-Q Advantage A10*, 18.2 MΩ / 25 °C, 2 ppb TOC) were used for mass spectrometry measurements.

3.2.2. Chemicals

Benzyl bromide (98%, Acros), 4-methoxybenzyl chloride (98%, Acros), 1-bromopropane (99%, Aldrich), 1-bromobutane (99%, Sigma), methyl bromoacetate (99%, Acros), ethyl bromoacetate (98%, Acros), sodium azide (≥ 99.0%, Fluka), copper(II)sulfate pentahydrate (≥ 99.0%, Fluka), phenylacetylene (98%, Aldrich), L(+)-ascorbic acid sodium salt (99.0%, Fluka), ruthenium(III) chloride hydrate (Johnson Matthey), alpha-terpinene (90%, Acros), sodium acetate anhydrous (≥ 98.5%, Fluka), molecular sieve (3 Å, beads, 4-8 mesh), phosphate buffered saline (pH 7.4, 10x, gibco), L-cysteine (Fluka), L-histidine (Merck) and L-methionine (Merck) were purchased from commercial suppliers and used without further purification.

3.3. General procedures

3.3.1. General procedure for the synthesis of triazole ligands

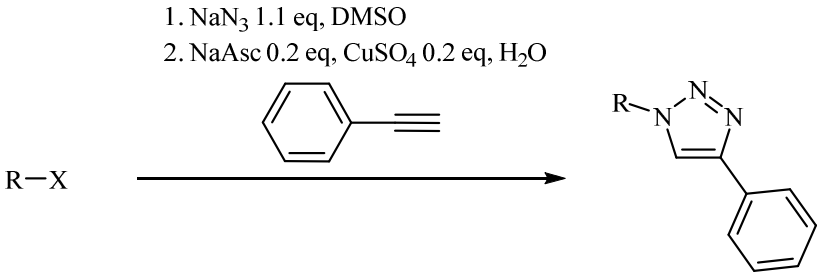

The respective organic halide (1.0 eq) was added to a solution of sodium azide (1.0 – 1.1 eq) in anhydrous DMSO (2 mL per mmol halide) and stirred at room temperature under argon atmosphere for 3 hours to a maximum of 3 days, depending on the utilized halide. Deionized water (2 mL per mmol halide) was added, followed by sodium ascorbate (0.2 eq), phenylacetylene (1.0 eq) and aqueous copper sulfate solution (1 M, 0.2 eq). The reaction mixture was stirred vigorously under inert conditions (6 hours to 2 days), followed by addition of water to complete precipitation of the product. The formed solid was collected by filtration, washed with water and purified by column chromatography to afford the desired triazole ligands **1a–f** in moderate to excellent yields (30 – 93%).

3.3.2. General procedure for the synthesis of Ru(II) cymene chloride complexes

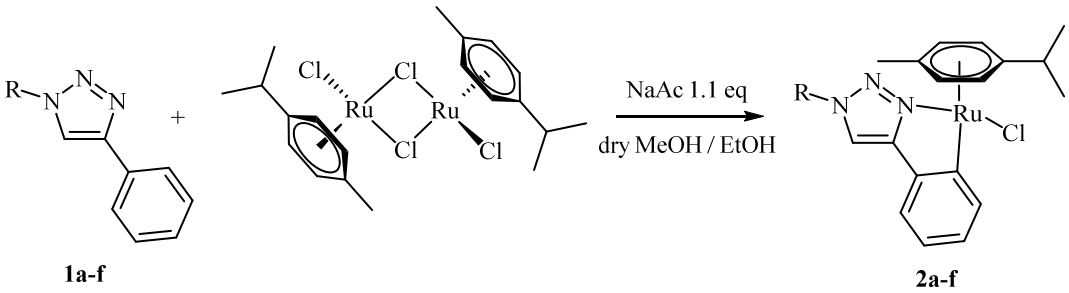

1a-f **2a-f**

Ligand **1a–f** (1.0 eq) and anhydrous sodium acetate (1.1 eq) were dissolved or suspended in methanol or ethanol (dried over molecular sieve, 3 Å) and stirred for 15 minutes under argon atmosphere. After addition of the ruthenium dimer (0.9 to 1.0 eq), the reaction mixture was stirred under inert conditions at room temperature for 16 hours to 5 days, during which time precipitation of the desired product occurred. Afterwards, the formed solid was filtered off and washed with small amounts of cold methanol or ethanol to remove excess ligand and dimer. The solid was dissolved in dichloromethane, filtered and evaporated to dryness or precipitated with *n*-hexane to afford the product **2a–f** as orange crystals in average to good yields (40 – 71%).

3.4. Ligand synthesis

3.4.1. 1-Benzyl-4-phenyl-*1H*-1,2,3-triazole **1a**

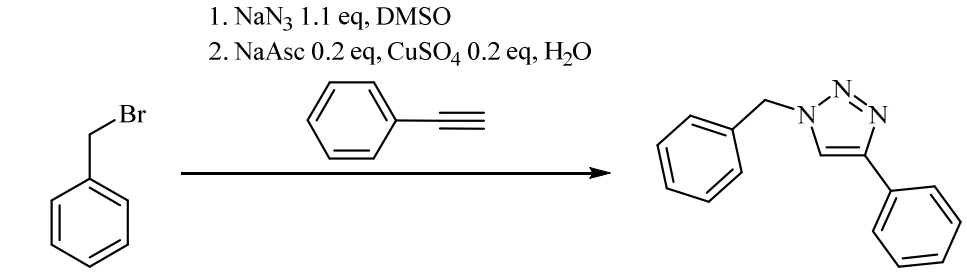

C_7H_7Br
M= 171.03 g/mol

$C_{15}H_{13}N_3$
M = 235.28 g/mol

The reaction was performed according to the general procedure for the synthesis of triazoles (see section 3.3.1), using benzyl bromide (1.42 mL, 12.0 mmol, 1.0 eq), sodium azide (859 mg, 13.2 mmol, 1.1 eq), sodium ascorbate (476 mg, 2.4 mmol, 0.2 eq), phenylacetylene (1.32 mL, 12.0 mmol, 1.0 eq) and copper(II)sulfate pentahydrate (600 mg, 2.4 mmol, 0.2 eq). After 3 hours of reaction time for the first step and 2.5 days for the second step, the obtained crude product was purified by column chromatography (10% acetone in chloroform, Silica 60), affording the desired product **1a** as colorless crystals.

Yield	2.64 g (93%)	
Melting point	126 – 130 °C	
Solubility	0.05 mg/mL ≡	0.21 mM
HRMS $[M+Na]^+$	258.1003	(found)
	258.1002	(calculated)

Elemental analysis

$C_{15}H_{13}N_3$	C [%]	H [%]	N [%]
calculated	76.57	5.57	17.86
found	76.32	5.20	17.66
Δ	0.25	0.37	0.20

NMR

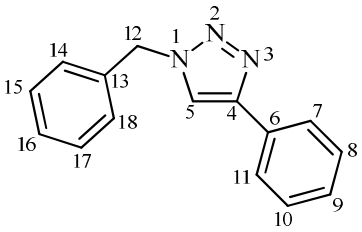

^{1}H NMR (500.10 MHz, 301 K, DMSO-d_6): δ = 8.63 (s, 1H, CH-5); 7.85 (d, ^{3}J(H,H) = 7 Hz, 2H, ArH-7/11); 7.44 (dd, ^{3}J(H,H) = 8 Hz, ^{3}J(H,H) = 8 Hz, 2H, ArH-8/10); 7.41 – 7.30 (m, 6H, ArH-9, ArH-14/18, ArH-15/17, ArH-16); 5.65 (s, 2H, CH_2-12) ppm.

^{13}C NMR (125.75 MHz, 304 K; DMSO-d_6): δ = 146.6 (C-4); 136.0 (C-13); 130.6 (C-6); 128.8 (CH-16, CH-8/10 or CH-15/17); 128.7 (CH-8/10 or CH-15/17); 128.1 (CH-9); 127.8 (CH-14/18); 125.1 (CH-7/11); 121.5 (CH-5); 53.0 (CH_2-12) ppm.

3.4.2. 1-(4-Methoxybenzyl)-4-phenyl-*1H*-1,2,3-triazole **1b**

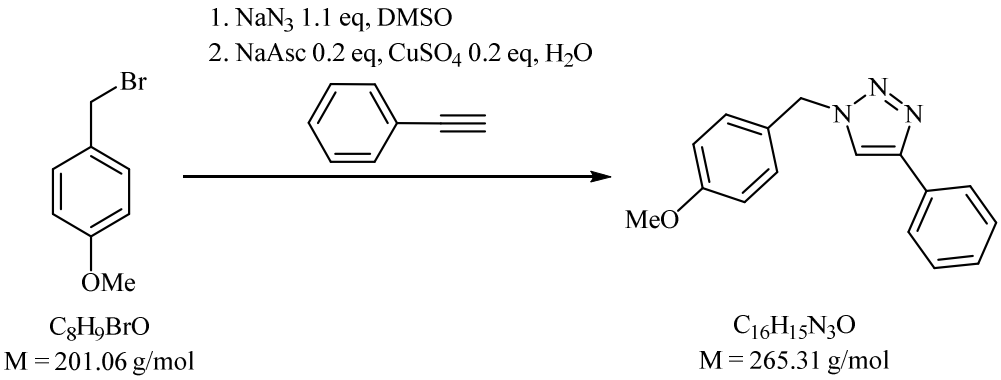

C_8H_9BrO
M = 201.06 g/mol

$C_{16}H_{15}N_3O$
M = 265.31 g/mol

The reaction was performed according to the general procedure for the synthesis of triazoles (see section 3.3.1), using 4-methoxybenzyl chloride (0.81 mL, 6.0 mmol, 1.0 eq), sodium azide (390 mg, 6.0 mmol, 1.0 eq), sodium ascorbate (240 mg, 1.2 mmol, 0.2 eq), phenylacetylene (0.66 mL, 6.0 mmol, 1.0 eq) and copper(II)sulfate pentahydrate (300 mg, 1.2 mmol, 0.2 eq). After 12 hours of reaction time for the first step and 6 hours for the second step, the obtained crude product was purified by column chromatography (5% acetone in chloroform, Silica 60), affording the desired product **1b** as colorless crystals.

Yield	864 mg (54%)	
Melting point	138 – 139 °C	
Solubility	0.09 mg/mL ≡ 0.34 mM	
HRMS [M+Na]$^+$	288.1102	(found)
	288.1107	(calculated)

Elemental analysis

$C_{16}H_{15}N_3O \cdot 0.1H_2O$	C [%]	H [%]	N [%]
calculated	71,94	5,74	15,73
found	72,12	5,68	15,46
Δ	0.18	0.06	0.27

NMR

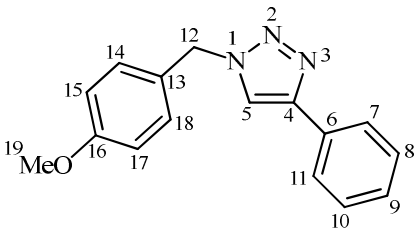

^{1}H NMR (500.10 MHz, 299 K, DMSO-d_6): δ = 8.58 (s, 1H, CH-5); 7.84 (d, ^{3}J(H,H) = 8 Hz, 2H, ArH-7/11); 7.43 (dd, ^{3}J(H,H) = 8 Hz, ^{3}J(H,H) = 8 Hz, 2H, ArH-8/10); 7.34 (d, ^{3}J(H,H) = 9 Hz, 2H, ArH-14/18); 7.31 (dd, ^{3}J(H,H) = 7 Hz, ^{3}J(H,H) = 7 Hz, 1H, ArH-9); 6.94 (d, ^{3}J(H,H) = 9 Hz, 2H, Ar-H); 5.56 (s, 2H, CH_2-12); 3.73 (s, 3H, CH_3-19) ppm.

^{13}C NMR (125.75 MHz, 300 K, DMSO-d_6): δ = 159.2 (C-16); 146.6 (C-4); 130.7 (C-6); 129.5 (CH-14/18); 128.8 (CH-8/10); 127.9 (C-13); 127.8 (CH-9); 125.1 (CH-7/11); 121.2 (CH-5); 114.1 (CH-15/17); 55.1 (CH_3-19); 52.6 (CH_2-12) ppm.

3.4.3. 4-Phenyl-1-propyl-*1H*-1,2,3-triazole **1c**

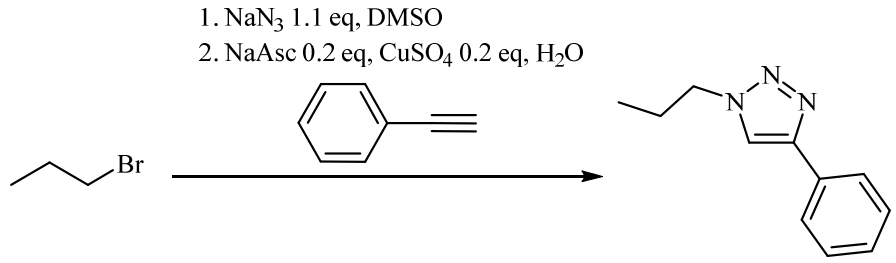

C_3H_7Br
M = 122.99 g/mol

$C_{11}H_{13}N_3$
M = 187.24 g/mol

The reaction was performed according to the general procedure for the synthesis of triazoles (see section 3.3.1), using 1-bromopropane (1.09 mL, 12.0 mmol, 1.0 eq), sodium azide (859 mg, 13.2 mmol, 1.0 eq), sodium ascorbate (476 mg, 2.4 mmol, 0.2 eq), phenylacetylene (1.32 mL, 12.0 mmol, 1.0 eq) and copper(II)sulfate pentahydrate (600 mg, 2.4 mmol, 0.2 eq). After 2 days of reaction time for the first step and 2 days for the second step, the obtained crude product was purified by column chromatography (5% acetone in chloroform, Silica 60), affording the desired product **1c** as colorless crystals.

Yield	674 mg (30%)	
Melting point	49 °C	
Solubility	0.67 mg/mL ≡ 3.58 mM	
HRMS $[M+Na]^+$	210.1002	(found)
	210.1002	(calculated)

Elemental analysis

$C_{11}H_{13}N_3$	C [%]	H [%]	N [%]
calculated	70.56	6.99	22.44
found	70.48	6.92	22.53
Δ	0.08	0.07	0.09

NMR

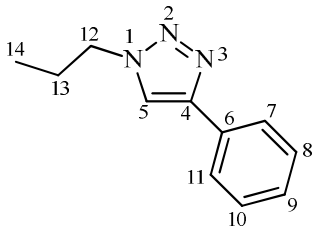

^{1}H NMR (500.10 MHz, 300 K, DMSO-d_6): δ = 8.59 (s, 1H, CH-5); 7.85 – 7.82 (m, 2H, ArH-7/11); 7.46 – 7.31 (m, 2H, ArH-8/10); 7.33 (dddd, , ^{3}J(H,H) = 9 Hz, ^{3}J(H,H) = 9 Hz, ^{4}J(H,H) = 1 Hz, , ^{4}J(H,H) = 1 Hz, 1H, ArH-9); 4.36 (t, ^{3}J(H,H) = 7 Hz, 2H, CH_2-12); 1.89 (sext, ^{3}J(H,H) = 7 Hz, 2H, CH_2-13); 0.88 (t, ^{3}J(H,H) = 7 Hz, 3H, CH_3-14) ppm.

^{13}C NMR (125.75 MHz, 300 K, DMSO-d_6): δ = 146.3 (C-4); 130.9 (C-6); 128.8 (CH-8/9); 127.7 (CH-9); 125.1 (CH-7/11); 121.2 (CH-5); 51.1 (CH_2-12); 23.1 (CH_2-13); 10.8 (CH_3-14) ppm.

3.4.4. 4-Phenyl-1-butyl-*1H*-1,2,3-triazole **1d**

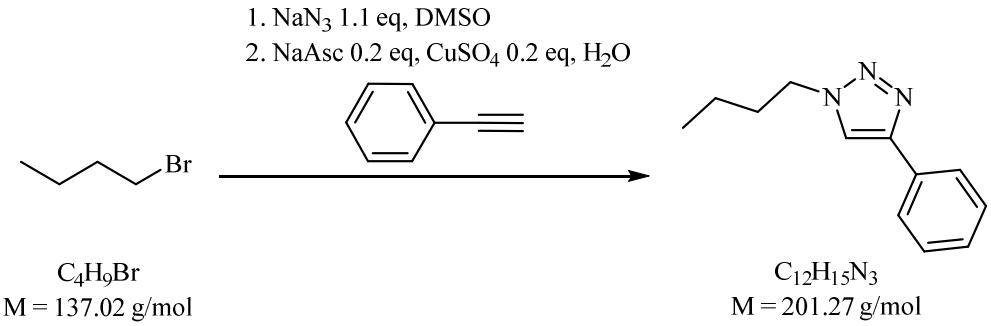

The reaction was performed according to the general procedure for the synthesis of triazoles (see section 3.3.1), using 1-bromobutane (0.32 mL, 3.0 mmol, 1.0 eq), sodium azide (195 mg, 3.0 mmol, 1.0 eq), sodium ascorbate (120 mg, 0.6 mmol, 0.2 eq), phenylacetylene (0.33 mL, 3.0 mmol, 1.0 eq) and copper(II)sulfate pentahydrate (150 mg, 0.6 mmol, 0.2 eq). After 24 hours of reaction time for the first step and 1.5 days for the second step, the obtained crude product was purified by column chromatography (10% acetone in chloroform, Silica 60), affording the desired product **1d** as colorless crystals.

Yield	413 mg (34%)	
Melting point	63 – 64 °C	
Solubility	0.34 mg/mL ≡ 1.69 mM	
HRMS [M+Na]$^+$	224.1159	(found)
	224.1158	(calculated)

Elemental analysis

$C_{12}H_{15}N_3$	C [%]	H [%]	N [%]
calculated	71.61	7.51	20.88
found	71.69	7.51	20.96
Δ	0.08	0.00	0.08

NMR

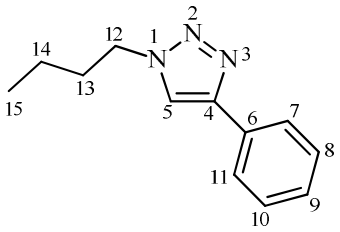

^{1}H NMR (500.10 MHz, 300 K, DMSO-d_6): δ = 8.57 (s, 1H, CH-5); 7.84 (d, ^{3}J(H,H) = 7 Hz, 3H, ArH-7/11); 7.44 (dd, ^{3}J(H,H) = 7 Hz, ^{3}J(H,H) = 7 Hz, 2H, ArH-8/10); 7.32 (dd, ^{3}J(H,H) = 7 Hz, ^{3}J(H,H) = 7 Hz, 1H, ArH-9); 4.39 (t, ^{3}J(H,H) = 7 Hz); 2H, CH2-12); 1.84 (quint, ^{3}J(H,H) = 7 Hz, 2H, ArH-13); 1.29 (sext, ^{3}J(H,H) = 7 Hz, 2H, ArH-14); 0.90 (t, ^{3}J(H,H) = 7 Hz, 3H, CH_3-15) ppm.

^{13}C NMR (125.75 MHz, 301 K, DMSO-d_6): δ = 146.2 (C-4); 130.9 (C-6); 128.8 (CH-8/10); 127.7 (CH-9); 125.0 (CH-7/11); 121.2 (CH-5); 49.2 (CH_2-12); 31.6 (CH_2-13); 19.1 (CH_2-14); 13.3 (CH_3-15) ppm.

3.4.5. Methyl[2-(4-phenyl-*1H*-1,2,3-triazol-1-yl)]acetate **1e**

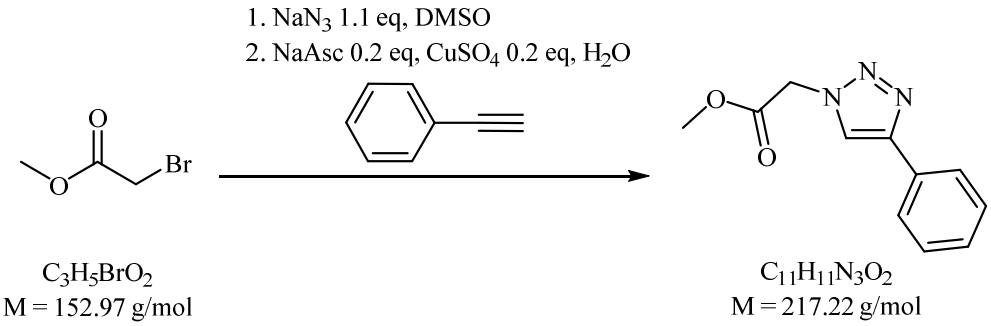

$C_3H_5BrO_2$
M = 152.97 g/mol

$C_{11}H_{11}N_3O_2$
M = 217.22 g/mol

The reaction was performed according to the general procedure for the synthesis of triazoles (see section 3.3.1), using methyl bromoacetate (1.14 mL, 12.0 mmol, 1.0 eq), sodium azide (859 mg, 13.2 mmol, 1.1 eq), sodium ascorbate (476 mg, 2.4 mmol, 0.2 eq), phenylacetylene (1.32 mL, 12.0 mmol, 1.0 eq) and copper(II)sulfate pentahydrate (600 mg, 2.4 mmol, 0.2 eq). After 5 days of reaction time for the first step and 2 days for the second step, the obtained crude product was purified by column chromatography (10% acetone in chloroform, Silica 60), affording the desired product **1e** as colorless crystals.

Yield	1.75 g (67%)	
Melting point	81 – 82 °C	
Solubility	1.05 mg/mL ≡ 4.83 mM	
HRMS [M+Na]$^+$	240.0747	(found)
	240.0743	(calculated)

Elemental analysis

$C_{11}H_{11}N_3O_2$	C [%]	H [%]	N [%]
calculated	60.81	5.11	19.35
found	60.72	4.89	19.26
Δ	0.09	0.22	0.09

NMR

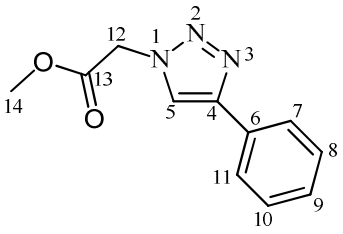

^{1}H NMR (500.10 MHz, 300 K, DMSO-d_6): δ = 8.56 (s, 1H, CH-5); 7.86 (d, ^{3}J(H,H) = 8 Hz, 2H, ArH-7/11); 7.46 (dd, ^{3}J(H,H) = 8 Hz, ^{3}J(H,H) = 8 Hz, 2H; ArH-8/10); 7.35 (dd, ^{3}J(H,H) = 8 Hz, ^{3}J(H,H) = 8 Hz, 1H, ArH-9); 5.48 (s, 2H, CH_2-12); 3.74 (s, 3H, CH_3-14) ppm.

^{13}C NMR (125.75 MHz, 301 K, DMSO-d_6): δ = 168.2 (C-13); 146.4 (C-4); 130.5 (C-6); 128.9 (CH-8/10); 128.0 (CH-9); 125.2 (CH-7/11); 122.7 (CH-5); 52.6 (CH_3-14); 50.4 (CH_2-12) ppm.

3.4.6. Ethyl[2-(4-phenyl-*1H*-1,2,3-triazol-1-yl)]acetate **1f**

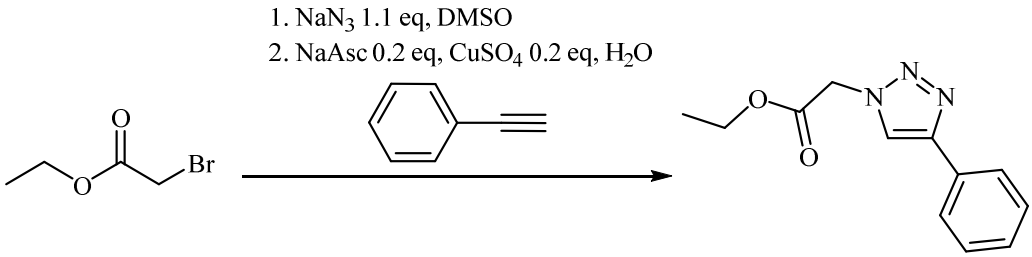

$C_4H_7BrO_2$
M = 167.00 g/mol

$C_{12}H_{13}N_3O_2$
M = 231.25 g/mol

The reaction was performed according to the general procedure for the synthesis of triazoles (see section 3.3.1), using ethyl bromoacetate (1.00 mL, 9.0 mmol, 1.0 eq), sodium azide (644 mg, 9.9 mmol, 1.1 eq), sodium ascorbate (350 mg, 1.8 mmol, 0.2 eq), phenylacetylene (0.99 mL, 9.0 mmol, 1.0 eq) and copper(II)sulfate pentahydrate (350 mg, 1.8 mmol, 0.2 eq). After 2 days of reaction time for the first step and 1.5 days for the second step, the obtained crude product was purified by column chromatography (5% acetone in chloroform, Silica 60), affording the desired product **1f** as colorless crystals.

Yield	1.84 g (88%)	
Melting point	99 – 100 °C	
Solubility	0.47 mg/mL ≡ 2.03 mM	
HRMS [M+Na]$^+$	254.0896	(found)
	254.0900	(calculated)

Elemental analysis

$C_{12}H_{13}N_3O_2$	C [%]	H [%]	N [%]
calculated	62.33	5.67	18.17
found	62.24	5.29	18.04
Δ	0.09	0.38	0.13

NMR

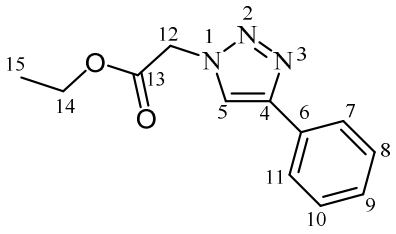

^{1}H NMR (500.10 MHz, 300 K, DMSO-d_6): δ = 8.56 (s, 1H, CH-5); 7.86 (d, ^{3}J(H,H) = 7 Hz, 2H, ArH-7/11); 7.46 (dd, ^{3}J(H,H) = 8 Hz, ^{3}J(H,H) = 8 Hz, 2H, ArH-8/10); 7.35 (dd, ^{3}J(H,H) = 7 Hz, ^{3}J(H,H) = 7 Hz, 1H, ArH-9); 5.45 (s, 2H, CH_2-12); 4.21 (q, ^{3}J(H,H) = 7 Hz, 2H, CH_2-14); 1.23 (t, ^{3}J(H,H) = 7 Hz, 3H, CH_3-15) ppm.

^{13}C NMR (125.75 MHz, 302 K; DMSO-d_6): δ = 167.2 (C-13); 146.4 (C-4); 130.5 (C-6); 128.9 (CH-8/10); 128.0 (CH-9); 125.2 (CH-7/11); 122.7 (CH-5); 61.6 (CH2-14); 50.6 (CH2-12); 14.0 (CH3-15) ppm.

3.5. Complex synthesis

3.5.1. Bis[(η^6-*p*-cymene)dichloridoruthenium]

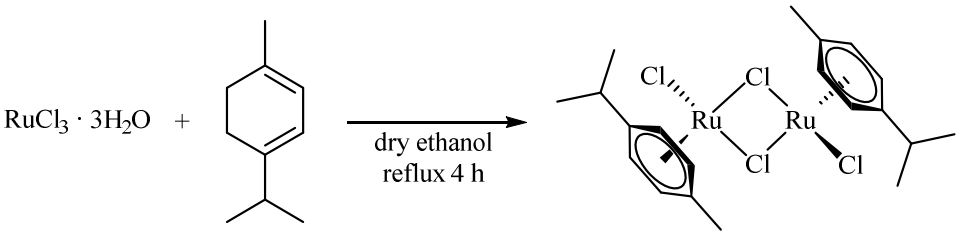

$C_{10}H_{16}$
M = 136,24

$C_{20}H_{28}Cl_4Ru_2$
M = 612.39

α-Terpinene (12.5 mL, 77 mmol) was added to a solution of $RuCl_3 \cdot 3H_2O$ (2.0 g, 7.6 mmol) in dry ethanol (75 mL) After heating to reflux for 4 hours, the reaction mixture was concentrated *in vacuo* to half of its original volume. Precipitation with diethyl ether afforded the product as red crystals, which were filtered off, washed with diethyl ether and dried *in vacuo*.

Yield 2.10 g (92%)

Melting point > 182 °C (decomposition)

NMR

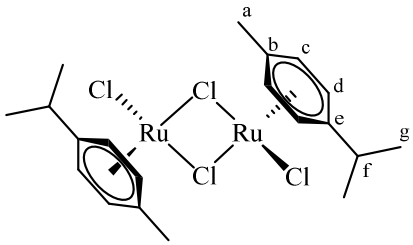

^{1}H NMR (500.10 MHz, 299 K, $CDCl_3$): δ = 5.47 (d, ^{3}J(H,H) = 6 Hz, 2H, ArH-c); 5.33 (d, ^{3}J(H,H) = 6 Hz, 2H, ArH-b); 2.92 (sept, ^{3}J(H,H) = 7 Hz, 1H, CH-f); 2.15 (s, 3H, CH_3-a); 1.28 (d, ^{3}J(H,H) = 7 Hz, 6H, CH_3-g) ppm.

^{13}C NMR (125.75 MHz, 298 K, $CDCl_3$): δ = 101.2 (C-e); 96.7 (C-b); 81.3 (CH-d); 80.5 (CH-c); 30.6 (CH-f); 22.2 (CH_3-g); 18.9 (CH_3-a) ppm.

3.5.2. [Chlorido(4-(2'-κC)-benzyl-1-butyl-*1H*-1,2,3-triazole-3-κN)(η^6-*p*-cymene)ruthenium(II)] **2a**

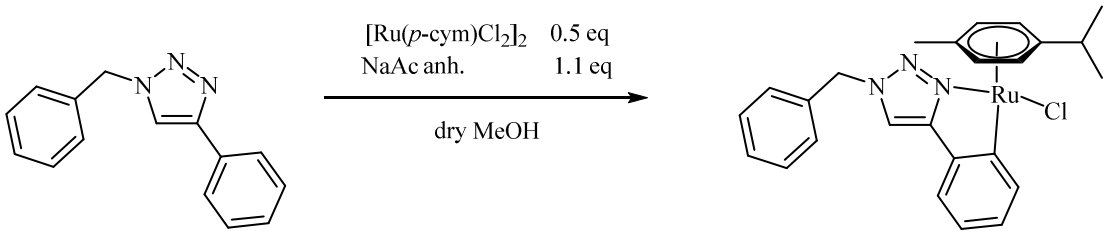

$C_{15}H_{13}N_3$
M = 235.28 g/mol
1a

$C_{25}H_{26}ClN_3Ru$
M = 505.02 g/mol
2a

The reaction was performed according to the general procedure for the synthesis of complexes (see section 3.3.2), using 1-benzyl-4-phenyl-*1H*-1,2,3-triazole (154 mg, 0.65 mmol, 1.0 eq), anhydrous sodium acetate (59 mg, 0.72 mmol, 1.1 eq) and bis[(η^6-p-cymene) dichloridoruthenium] (200 mg, 0.33 mmol, 1.0 eq) in dry methanol (10 mL) for a reaction time of 5 days, affording the complex **2a** as orange crystals.

Yield	231 mg (70%)	
Melting point	230 – 239 °C (decomposition)	
Solubility	0.02 mg/mL ≡ 0.04 mM	
HRMS [M-Cl]$^+$	470.1184	(found)
	470.1164	(calculated)

Elemental analysis

$C_{25}H_{26}ClN_3Ru$	C [%]	H [%]	N [%]
calculated	59.46	5.19	8.32
found	59.45	4.94	8.35
Δ	0.01	0.25	0.03

NMR

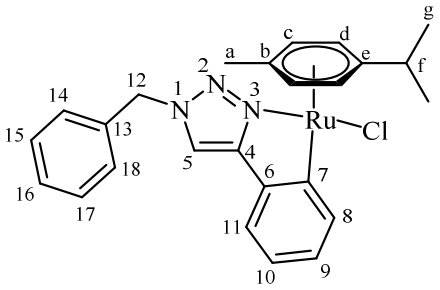

^{1}H NMR (500.10 MHz, 299 K, $CDCl_3$): δ = 8.15 (d, ^{3}J(H,H) = 7 Hz, 1H, ArH-8); 7.52 (s, 1H, CH-5); 7.36 – 7.31 (m, 3H, ArH-14/18, ArH-16); 7.25 – 7.22 (m, 2H, ArH-15/17); 7.21 (dd, ^{3}J(H,H) = 7 Hz, ^{4}J(H,H) = 1 Hz, 1H, ArH-11); 7.10 (ddd, ^{3}J(H,H) = 7 Hz, ^{3}J(H,H) = 7 Hz, ^{4}J(H,H) = 1 Hz, 1H, ArH-9); 6.97 (ddd, ^{3}J(H,H) = 7 Hz, ^{3}J(H,H) = 7 Hz, ^{4}J(H,H) = 1 Hz, ArH-10); 5.55 (d, ^{3}J(H,H) = 6 Hz, 1H, ArH-c_1); 5.49 (d, ^{3}J(H,H) = 6 Hz, 1H, ArH-d_1); 5.46 (d, ^{3}J(H,H) = 6 Hz, 1H, ArH-d_2); 5.40 (d, ^{1}J(H,H) = 15 Hz, 1H, ArH-12_a); 5.25 – 5.20 (m, 2H, CH-12_b, ArH-c_2); 2.40 (sept, ^{3}J(H,H) = 7 Hz, CH-f); 2.03 (s, 3H, CH_3-a); 0.92 (d, ^{3}J(H,H) = 7 Hz, CH_3-g_1); 0.85 (d, ^{3}J(H,H) = 7 Hz, CH_3-g_2) ppm.

^{13}C NMR (125.75 MHz, 301 K, $CDCl_3$): δ = 176.3 (C-7); 155.6 (C-4); 139.7 (CH-8); 135.3 (C-6); 134.5 (C-13); 129.2 (CH-15/17); 128.9 (CH-16); 128.2 (CH-14/18); 127.8 (CH-9); 122.8 (CH-10); 122.4 (CH-11); 117.4 (CH-5); 99.6 (C-e); 98.8 (C-b); 89.1 (C-c_1); 87.4 (C-d_2); 85.6 (C-d_1); 83.5 (C-c_2), 55.0 (CH_2-12); 30.9 (CH-f); 22.3 (CH3-g_1); 22.2 (CH_3-g_1); 18.9 (CH_3-a) ppm.

3.5.3. [Chlorido(4-(2'-κC)-phenyl-1-(4-methoxybenzyl)-*1H*-1,2,3-triazole-3-κN)(η^6-*p*-cymene)ruthenium(II)] **2b**

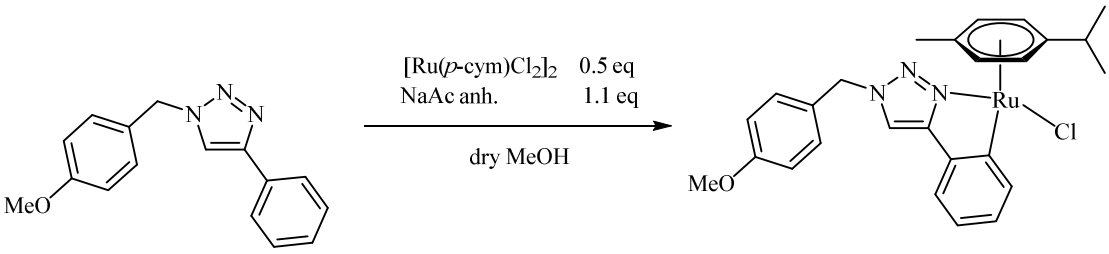

$C_{16}H_{15}N_3O$
M = 265.31 g/mol
1b

$C_{26}H_{28}ClN_3ORu$
M = 535.04 g/mol
2b

The reaction was performed according to the general procedure for the synthesis of complexes (see section 3.3.2), using 1-(4-methoxybenzyl)-4-phenyl-*1H*-1,2,3-triazole (173 mg, 0.65 mmol, 1.0 eq) and sodium acetate (59 mg, 0.72 mmol, 1.1 eq) and bis[(η^6-*p*-cymene)dichloridoruthenium] (200 mg, 0.33 mmol, 1.0 eq) in dry methanol (10 mL) for a reaction time of 5 days, affording the complex **2b** as orange crystals.

Yield	214 mg (61%)	
Melting point	235 – 245 °C (decomposition)	
Solubility	0.04 mg/mL ≡ 0.07 mM	
HRMS [M-Cl]$^+$	500.1292	(found)
	500.1270	(calculated)

Elemental analysis

$C_{26}H_{28}ClN_3ORu$	C [%]	H [%]	N [%]	S [%]
calculated	58.37	5.27	7.85	0.00
found	58.32	5.35	8.18	< 0.02
Δ	0.05	0.08	0.33	< 0.02

NMR

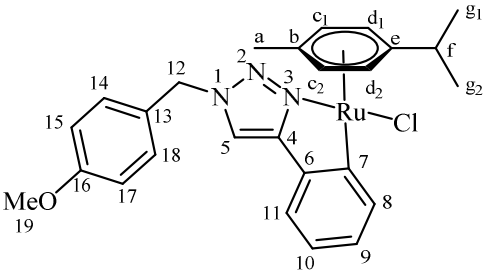

^{1}H NMR (500.10 MHz, 299 K, $CDCl_3$): δ = 8.14 (d, ^{3}J(H,H) = 7 Hz, 1H, ArH-8); 7.39 (s, 1H, CH-5); 7.09 (ddd, ^{3}J(H,H) = 7 Hz, ^{3}J(H,H) = 7 Hz, ^{4}J(H,H) = 1 Hz, 1H, ArH-9); 7.25 – 7.21 (m, 3H, ArH-11, ArH-14/18); 6.94 (dd, ^{3}J(H,H) = 7 Hz, ^{3}J(H,H) = 7 Hz, 1H, ArH-10); 6.92 – 6.89 (m, 2H, ArH-15/17); 5.56 (d, ^{3}J(H,H) = 6 Hz, 1H, ArH-c_1); 5.53 – 5.46 (m, 2H, ArH-d_1, ArH-d_2); 5.50 (d, ^{2}J(H,H) = 15 Hz, 1H, CH_2-12_a); 5.37 (d, ^{3}J(H,H) = 15 Hz, 1H, CH_2-12_b); 5.21 (d, ^{3}J(H,H) = 6 Hz, ArH-c_2), 3.81 (s, 3H, OCH_3-19); 2.45 (sept, ^{3}J(H,H) = 7 Hz, 1H, CH-f); 2.04 (s, 3H, ArH-a); 0.95 (d, ^{3}J(H,H) = 7 Hz, 3H, CH_3-g_1); 0.90 (d, ^{3}J(H,H) = 7 Hz, 3H, CH_3-g_2) ppm.

^{13}C NMR (125.81 MHz, 300 K, $CDCl_3$): δ = 176.3 (C-7); 160.1 (C-16); 155.4 (C-4); 139.6 (C-8); 135.3 (C-6); 129.9 (CH-14/18); 127.7 (CH-9); 126.4 (C-13); 122.7 (CH-10); 122.4 (CH-11); 117.2 (CH-5); 114.5 (CH-15/17); 99.6 (C-e); 98.7 (C-b); 89.0 (CH-c_1); 87.4 (CH-d_2); 85.5 (CH-d_1); 83.5 (CH-c_2); 55.5 (CH_3-19); 54.5 (CH_2-12); 30.8 (CH-f); 22.3 (CH_3-g_1); 22.2 (CH_3-g_2); 18.8 (CH_3-a) ppm.

3.5.4. [Chlorido(4-(2'-*κ*C)-phenyl-1-propyl-*1H*-1,2,3-triazole-3-*κ*N)(η^6-*p*-cymene)ruthenium(II)] **2c**

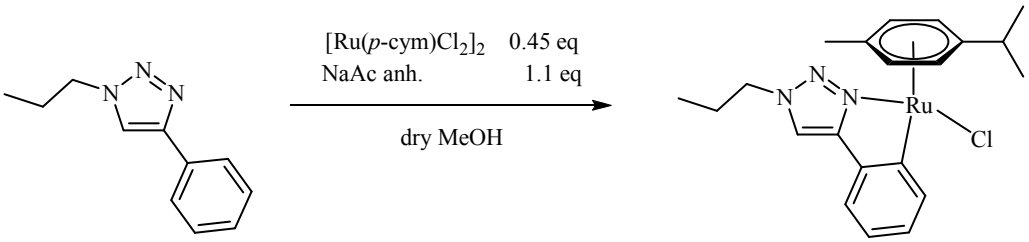

$C_{11}H_{13}N_3$
M = 187.24 g/mol
1c

$C_{21}H_{26}ClN_3Ru$
M = 456.97g/mol
2c

The reaction was performed according to the general procedure for the synthesis of complexes (see section 3.3.2) using 4-phenyl-1-propyl-*1H*-1,2,3-triazole (136 mg, 0.73 mmol, 1.0 eq), sodium acetate (66 mg, 0.80 mmol, 1.1 eq) and bis[(η^6-*p*-cymene)dichloridoruthenium] (200 mg, 0.33 mmol, 0.9 eq) in dry methanol (5 mL) for a reaction time of 5 days, affording the complex **2c** as orange crystals.

Yield	114 mg (40%)	
Melting point	212 – 220 °C (decomposition)	
Solubility	0.05 mg/mL ≡ 0.11 mM	
HRMS [M-Cl]$^+$	422.1176	(found)
	422.1164	(calculated)

Elemental analysis

$C_{21}H_{26}ClN_3Ru \cdot 0.6H_2O$	C [%]	H [%]	N [%]	S [%]
calculated	53.91	5.86	8.98	0.00
found	53.67	5.65	8.99	< 0.02
Δ	0.24	0.21	0.01	< 0.02

NMR

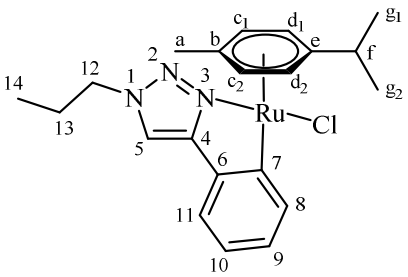

^{1}H NMR (500.32 MHz, 300 K, $CDCl_3$): δ = 8.15 (d, ^{3}J(H,H) = 7 Hz, 1H, ArH-8); 7.55 (s, 1H, CH-5); 7.24 (d, ^{3}J(H,H) = 7 Hz, 1H, ArH-11); 7.10 (dd, ^{3}J(H,H) = 7 Hz, ^{3}J(H,H) = 7 Hz, 1H, ArH-9); 6.97 (dd, ^{3}J(H,H) = 7 Hz, ^{3}J(H,H) = 7 Hz, 1H, ArH-10); 5.54 (d, ^{3}J(H,H) = 6 Hz, 1H, ArH-c_1); 5.49 (d, ^{3}J(H,H) = 6 Hz, 1H, ArH-d_2); 5.45 (d, ^{3}J(H,H) = 6 Hz, 1H, ArH-d_2); 5.20 (d, ^{3}J(H,H) = 6 Hz, 1H, ArH-c_2); 4.27 – 4.04 (m, 2H, CH_2-12); 2.42 (sept, ^{3}J(H,H) = 7 Hz, 1H, CH-f); 2.03 (s, 3H, CH_3-a); 1.94 – 1.83 (m, 2H, CH_2-13); 0.95 – 0.89 (m, 9H, ArH-g_1; ArH-g_2, CH_3-14) ppm.

^{13}C NMR (125.81 MHz, 301 K, $CDCl_3$): δ = 176.2 (C-7); 155.2 (C-4); 139.6 (CH-8); 135.4 (C-6); 127.7 (CH-9); 122.7 (CH-10); 122.3 (CH-11); 117.2 (CH-5); 99.4 (C-e); 99.1 (C-b); 88.8 (CH-c_1); 87.8 (CH-d_2); 85.2 (CH-d_1); 83.2 (CH-c_2); 53.1 (CH_2-12); 30.9 (CH-f); 23.6 (CH-13); 22.4 (CH_3-g_1); 22.1 (CH_3-g_2); 18.9 (CH_3-a); 11.0 (CH_3-14) ppm.

3.5.5. [Chlorido(4-(2'-*κ*C)-phenyl-1-butyl-*1H*-1,2,3-triazole-3-*κ*N)(η^6-*p*-cymene)ruthenium(II)] **2d**

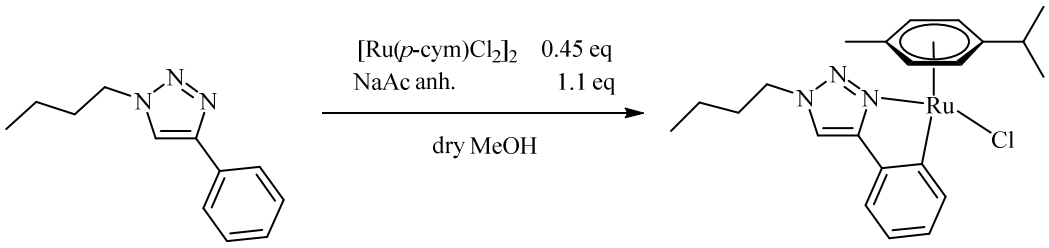

$C_{12}H_{15}N_3$
M = 201.27 g/mol
1d

$C_{22}H_{28}ClN_3Ru$
M = 471.00g/mol
2d

The reaction was performed according to the general procedure for the synthesis of complexes (see section 3.3.2) using 1-butyl-4-phenyl-1H-1,2,3-triazole (146 mg, 0.73 mmol, 1.0 eq), sodium acetate (65 mg, 0.80 mmol, 1.1 eq) and bis[(η^6-*p*-cymene)dichloridoruthenium] (200 mg, 0.33 mmol, 0.9 eq) in dry methanol (5 mL) for a reaction time of 16 hours, affording the complex **2d** as orange crystals.

Yield	186 mg (60%)	
Melting point	212 – 220 °C (decomposition)	
Solubility	0.02 mg/mL ≡ 0.05 mM	
HRMS [M-Cl]$^+$	436.1326	(found)
	436.1321	(calculated)

Elemental analysis

$C_{22}H_{28}ClN_3Ru \cdot 0.5H_2O$	C [%]	H [%]	N [%]	S [%]
calculated	55.04	6.09	8.75	0.00
found	54.94	5.85	8.54	< 0.02
Δ	0.10	0.24	0.21	< 0.02

NMR

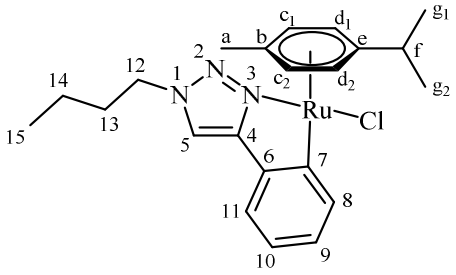

^{1}H NMR (500.32 MHz, 300 K, $CDCl_3$): δ = 8.14 (d, ^{3}J(H,H) = 7 Hz, 1H, ArH-8); 7.55 (s, 1H, CH-5); 7.22 (d, ^{3}J(H,H) = 7 Hz, 1H, ArH-11); 7.09 (dd, ^{3}J(H,H) = 7 Hz, ^{3}J(H,H) = 7 Hz, 1H, ArH-9); 6.97 (dd, ^{3}J(H,H) = 7 Hz, ^{3}J(H,H) =7 Hz, 1H, ArH-10); 5.53 (d, ^{3}J(H,H) = 6 Hz, 1H, ArH-c_1); 5.48 (d, ^{3}J(H,H) = 6 Hz, 1H, ArH-d_2); 5.45 (d, ^{3}J(H,H) = 6 Hz, 1H, ArH-d_1); 5.20 (d, ^{3}J(H,H) = 6 Hz, 1H, ArH-c_2); 4.27 – 4.19 (m, 1H, CH2-12$_a$); 4.08 – 4.00 (m, 1H, CH2-12$_b$); 2.41 (sept, ^{3}J(H,H) = 7 Hz, 1H, CH-f); 2.02 (s, 3H, CH_3-a); 1.81 (quint, ^{3}J(H,H) = 7 Hz, 2H, CH_2-13); 1.32 – 1.22 (m, 2H, CH_2-14); 0.95 – 0.88 (m, 9H, CH_3-g_1, CH_3-g_2, CH_3-15) ppm.

^{13}C NMR (125.81 MHz, 301 K, $CDCl_3$): δ = 176.2 (C-7); 155.2 (C-4); 139.6 (C-8); 135.4 (C-6); 127.6 (CH-9); 122.7 (CH-10); 122.3 (CH-11); 117.3 (CH-5); 99.4 (C-e); 99.0 (C-b); 88.8 (CH-c_1); 87.7 (CH-d_2); 85.3 (CH-d_1); 83.3 (CH-c_2); 51.2 (CH-12); 32.1 (CH_2-13); 30.9 (CH-f); 22.4 (CH_3-g_1); 22.1 (CH_3-g_2); 19.7 (CH_2-14); 18.8 (CH_3-a); 13.5 (CH_3-15) ppm.

3.5.6. [Chlorido(methyl-2-(4-(2'-κC)-phenyl-*1H*-1,2,3-triazol-(3-κN)-1-yl)acetate)(η^6-*p*-cymene)ruthenium(II)] **2e**

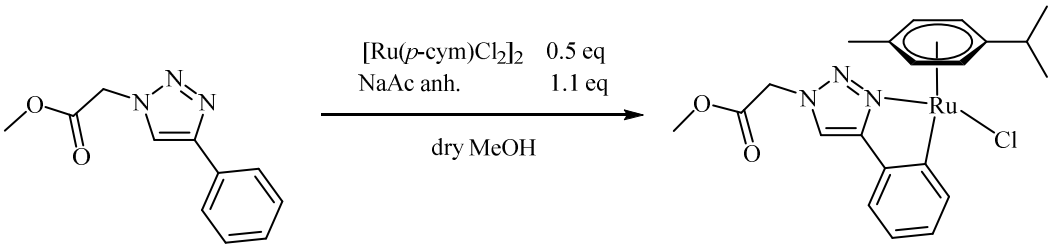

$C_{11}H_{11}N_3O_2$
M = 217.22 g/mol
1e

$C_{21}H_{24}ClN_3O_2Ru$
M = 486.96 g/mol
2e

The reaction was performed according to the general procedure for the synthesis of complexes (see section 3.3.2) using methyl 2-(4-phenyl-*1H*-1,2,3-triazol-1-yl)acetate (158 mg, 0.73 mmol, 1.0 eq), sodium acetate (65 mg, 0.80 mmol, 1.1 eq) and bis[(η^6-*p*-cymene)dichloridoruthenium] (200 mg, 0.33 mmol, 0.9 eq) in dry methanol (5 mL) for a reaction time of 16 hours, affording the complex **2e** as orange crystals.

Yield	148 mg (42%)	
Melting point	235 – 242 °C (decomposition)	
Solubility	0.11 mg/mL ≡ 0.22 mM	
HRMS [M-Cl]$^+$	452.0914	(found)
	452.0906	(calculated)

Elemental analysis

$C_{21}H_{24}ClN_3O_2Ru \cdot 0.5\ H_2O$	C [%]	H [%]	N [%]	S [%]
calculated	50.80	5.08	8.47	0.00
found	51.04	4.94	8.55	< 0.02
Δ	0.24	0.14	0.08	< 0.02

NMR

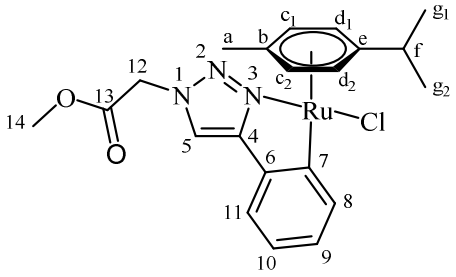

^{1}H NMR (500.10 MHz, 300 K, $CDCl_3$): δ = 8.16 (d, ^{3}J(H,H) = 7 Hz, 1H, ArH-8); 7.74 (s, 1H, CH-5); 7.19 – 7.12 (m, 2H, ArH-9, ArH-11); 7.01 (dd, ^{3}J(H,H) = 7 Hz, ^{3}J(H,H) = 7 Hz, 1H, ArH-10); 5.51 (d, ^{3}J(H,H) = 6 Hz, 1H, ArH-c_1); 5.47 (d, ^{3}J(H,H) = 6 Hz, 1H, ArH-d_2); 5.44 (d, ^{3}J(H,H) = 6 Hz, 1H, ArH-d_1); 5.20 (d, ^{3}J(H,H) = 6 Hz, 1H, ArH-c_2); 4.62 (d, ^{2}J(H,H) = 18 Hz, 1H, CH_2-12_a); 4.53 (d, ^{2}J(H,H) = 18 Hz, 1H, CH_2-12_b); 3.67 (s, 3H; CH_3-14); 2.35 (sept, ^{3}J(H,H) = 7 Hz; 1H, CH-f); 1.98 (s, 3H, CH_3-a); 0.92 (d, ^{3}J(H,H) = 7 Hz, 3H, CH_3-g_1); 0.87 (d, ^{3}J(H,H) = 7 Hz, 3H, CH_3-g_2) ppm.

^{13}C NMR (125.75 MHz, 300 K, $CDCl_3$): δ = 176.2 (C-7); 166.9 (C-13); 154.9 (C-3); 139.9 (CH-8); 135.3 (CH-6); 127.7 (CH-9); 122.7 (CH-10); 122.4 (CH-11); 119.8 (CH-5); 99.5 (C-e); 99.1 (C-b); 88.9 (CH-c_1); 88.0 (CH-d_2); 85.5 (C-d_1); 83.3 (C-c_2); 52.9 (CH_2-14); 50.9 (CH_2-12); 30.8 (CH-f); 22.31 (CH_3-g_1); 22.1 (CH_3-g_2); 18.7 (CH_3-a) ppm.

3.5.7. [Chlorido(ethyl-2-(4-(2'-*κ*C)-phenyl-*1H*-1,2,3-triazol-(3-*κ*N)-1-yl)acetate)(η^6-*p*-cymene)ruthenium(II)] **2f**

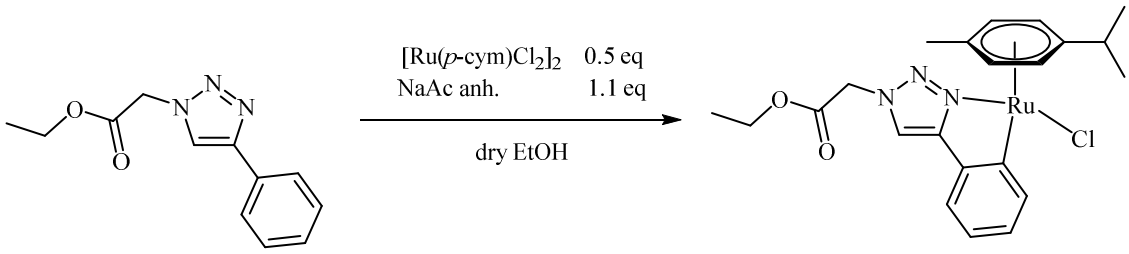

$C_{12}H_{13}N_3O_2$
M = 231.25 g/mol
1f

$C_{22}H_{26}ClN_3O_2Ru$
M = 500.98 g/mol
2f

The reaction was performed according to the general procedure for the synthesis of complexes (see section 3.3.2) using ethyl 2-(4-phenyl-*1H*-1,2,3-triazol-1-yl)acetate (151 mg, 0.65 mmol, 1.0 eq), sodium acetate (59 mg, 0.72 mmol, 1.1 eq) and bis[(η^6-*p*-cymene)dichloridoruthenium] (200 mg, 0.33 mmol, 1.0 eq) in dry ethanol (5 mL) for a reaction time of 2 days, affording the complex **2f** as orange crystals.

Yield	230 mg (71%)	
Melting point	237 – 240 °C (decomposition)	
Solubility	0.11 mg/mL ≡ 0.22 mM	
HRMS [M-Cl]$^+$	466.1060	(found)
	466.1063	(calculated)

Elemental analysis

$C_{22}H_{26}ClN_3O_2Ru$	C [%]	H [%]	N [%]	S [%]
calculated	52.74	5.23	8.39	0.00
found	52.65	4.89	8.33	< 0.02
Δ	0.09	0.34	0.06	< 0.02

NMR

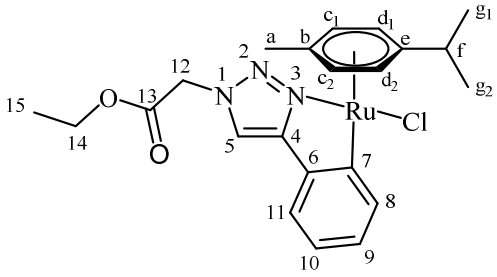

^{1}H NMR (500.10 MHz, 300 K, $CDCl_3$): δ = 8.17 – 8.14 (m, 1H, ArH-8); 7.75 (s, 1H; CH-5); 7.15 – 7.11 (m, 2H; ArH-9; ArH-11); 7.00 (dd, ^{3}J(H,H) = 7 Hz, ^{3}J(H,H) = 7^{3}J(H,H) = 6 Hz, 1H, ArH-c_1); 5.47 ^{3}J(H,H) = 6 Hz, 1H, ArH-d_2); 5.43 ^{3}J(H,H) = 6 Hz, 1H, ArH-d_1); 5.19 ^{3}J(H,H) = 6 Hz, 1H, ArH-c_2); 4.56 (d, ^{2}J(H,H) = 18 Hz; 1H, CH_2-12_a); 4.43 (d, ^{2}J(H,H) = 18 Hz; 1H, CH_2-12_b); 4.16 – 4.06 (m, 2H, CH_2-14); 2.33 (sept, ^{3}J(H,H) = 7 Hz, 1H, CH-f); 1.97 (s, 3H, CH_3-a); 1.20 (t, ^{3}J(H,H) = 7 Hz, 3H, CH_3-15); 0.90 (d, ^{3}J(H,H) = 7 Hz, 3H, CH_3-g_1); 0.86 (d, ^{3}J(H,H) = 7 Hz, 3H, CH_3-g_2) ppm.

^{13}C NMR (125.75 MHz. 301 K, $CDCl_3$): δ = 176.1 (C-7); 166.4 (C-13); 154.7 (C-4); 139.8 (CH-8); 135.5 (C-6); 127.6 (CH-9); 122.8 (CH-10); 122.4 (CH-11); 120.1 (CH-5); 99.3 (C-e); 99.1 (C-b); 88.7 (C-c_1); 88.1 (C-d_2); 85.4 (C-d_1); 83.3 (C-c_2); 62.1 (CH_2-14); 51.1 (CH_2-12); 30.7 (CH-f); 22.3 (CH_3-g_1); 22.0 (CH_3-g_2); 18.7 (CH_3-a); 14.1 (CH_3-15) ppm.

4. CONCLUSION AND OUTLOOK

Over the course of this master thesis, six different 1-substituted 4-phenyl-1,2,3-triazoles were synthesized in average to excellent yields. Subsequently, a synthetic procedure for the generation of *N*,*C*-coordinated triazoles bearing organometallic ruthenium(II)–arene fragments was developed. Six corresponding *N*,*C*-coordinated ruthenium(II) complexes were synthesized in average to good yields. Ligands and complexes were characterized via ^{1}H-, ^{13}C- and two-dimensional NMR techniques, X-ray diffraction analyses, high-resolution mass spectrometry, elemental analyses and melting point measurements. All complexes exhibited poor solubility in PBS and hydrolyzed rapidly in aqueous media as indicated by ESI-MS investigations. In biomolecule binding studies, no amino acid adducts were observed, accounting for the strong *N*,*C*-coordination between metal and the triazole chelate.

The performed research established a synthetic pathway for the development of *N*,*C*-coordinated triazole bearing ruthenium(II) arene complexes. Due to similarity to ruthenium, osmium(II)-arene complexes, analogous to the compounds presented in this thesis, can likely be synthesized in a similar way and evaluated in biological assays. The synthesis of other *N*,*C*-coordinated platinum metal arene complexes (Rh, Ir) is subject for further investigations.

Preliminary biological screening results indicate promising activity in the low micromolar range. In-depth analysis of the antiproliferative activity of the complexes and improvement of triazole substitution according to the obtained results remains a topic for future research.

The abundance of diverse starting materials, strength of the metal-ligand bond, robustness of the synthetic pathway, potential introduction of functional groups with targeting properties and high adjustability render this newly explored compound class a desirable and exciting ligand scaffold for the future development of anticancer agents.

5. REFERENCES

[1] Boyle, P.; Levin, B. *World Cancer Report* **2008**, 13.

[2] http://www.statistik.at/web_de/statistiken/gesundheit/todesursachen/todesursachen_im_ueberblick/index.html (Retrieved: 04-01-2014)

[3] http://www.cancerresearchuk.org/about-cancer/cancers-in-general/cancer-questions/how-many-different-types-of-cancer-are-there (Retrieved: 04-01-2014)

[4] http://www.statistik.at/web_de/statistiken/gesundheit/krebserkrankungen/krebs_gesamt/index.html (Retrieved: 04-01-2014)

[5] Khatib, O.; Aljurf, M. *Hematol. Oncol. Stem Cell Ther.* **2008**, 1, 44-52.

[6] Lutz, W. K.; Fekete, T. *Int. Arch. Occ. Env. Hea.* **1996**, 68, 120-125.

[7] Graphic originally published in Hanahan, D.; Weinberg, R. A. *Cell* **2011**, 144, 646-674., Elsevier user license applies.

[8] Ciardiello, E.; Kim, N.; McGeady, M. L.; Liscia, D. S.; Saeki, T.; Bianco, C.; Salomon, D. S. *Ann. Oncol.* **1991**, 2, 169-182.

[9] Yu, D.; Hung, M.-C. *Oncogene* **200**, 19, 6115-6121

[10] Jakowlew, S. B. *Cancer Metast. Rev.* **2006**, 25, 435-457.

[11] Muller, P. A. J.; Vousden, K. H. *Nat. Cell Biol.* **2013**, 15, 2-8.

[12] Shay, J. W.; Zou, Y.; Hiyama, E.; Wright, W. E. *Hum. Mol. Gen.* **2001**, 10, 677-685.

[13] Flamme, I.; Frölich, T.; Risau, W. *J. Cell. Physiol.* **1997**, 173, 206-210.

[14] Gilkes, D. M.; Semenza, G. L.; Wirtz, D. *Nat. Rev. Cancer* **2014**, 14, 430-439.

[15] Clark, W. H. *Br. J. Cancer* **1991**, 64, 631-644.

[16] Jordan, V. C. *Eur. J. Cancer* **2008**, 44, 30-38.

[17] http://www.cancer.org/treatment/treatmentsandsideeffects/treatmenttypes/chemotherapy/chemotherapyprinciplesanin-depthdiscussionofthetechniquesanditsroleintreatment/chemotherapy-principles-types-of-chemo-drugs (Retrieved: 26-12-2014)

[18] Parker, W. B. *Chem. Rev.* **2009**, 109, 2880-2893.

[19] Heidelberger, C.; Chaudhuri, N. K.; Danneberg, P.; Mooren, D.; Griesbach, L.; Duschinsky, R.; Schnitzer, R. J.; Pleven, E.; Scheiner, J. *Nature* **1957**, 179, 663-666.

[20] Adams, D. J.; Wahl, M. L.; Flowers, J. L.; Sen, B.; Colvin, M.; Dewhirst, M. W.; Manikumar, G.; Wani, M. C. *Cancer Chemother. Pharmacol.* **2006**, 57, 145-154.

[21] Pommier, Y.; Leo, E.; Zhang, H.; Marchand, C. *Chem. Biol.* **2010**, 17, 421-433.

[22] Chabner, B. A. *Cancer Res.* **2010**, 70, 428-429.

[23] Peters, J. A.; Huskens, J.; Raber, D. J. *Progress in Nuclear Magnetic Resonance Spectroscopy* **1996**, 28, 283-350.

[24] Caravan, P.; Ellison, J. J.; McMurry, T. J.; Lauffer, R. B. *Chem. Rev.* **1999**, 99, 2293-2352.

[25] Friederich, J. A.; Butterworth, J. F. *Anesthesia & Analgesia* **1995**, 81, 152-162.

[26] McNeill, J. H.; Yuen, V. G.; Hoveyda, H. R.; Orvig, C. *J. Med. Chem.* **1992**, 35, 1489-1491.

[27] Rosenberg, B.; Van Kamp, L.; Krigas, T. *Nature* **1965**, 205, 698-699.

[28] Rosenberg, B.; Van Kamp, L.; Trosko, J. E.; Mansour, V. H. *Nature* **1969**, 222, 385-386.

[29] Einhorn, L. H.; Donohue, *J. Ann. Intern. Med.* **1977**, 87, 293-298.

[30] Cepeda, V.; Fuertes, M. A.; Castilla, J.; Alonso, C.; Quevedo, C.; Pérez, J. M. *Anti-Cancer Agents Med. Chem.* **2007**, 7, 3-18.

[31] Kidani, Y.; Inagaki, K.; Iigo, M.; Hoshi, A.; Kuretani, K. *J. Med. Chem.* **1978**, 21, 1315-1318.
[32] Ishida, S.; Lee, J.; Thiele, D. J.; Herskowitz, I. *Proc. Natl. Acad. Sci. USA* **2002**, 99, 14298-14302.
[33] Reedijk, *J. Proc. Acad. Natl. Sci.* **2003**, 100, 3611-3616.
[34] Pongratz, M.; Schluga, P.; Jakupec, M. A.; Arion, V. B.; Hartinger, C. G.; Allmaier, G.; Keppler, B. K. *J. Anal. At. Spectrom.* **2004**, 19, 46-51.
[35] Pluim, D.; Waardenburg, R. C. A. M. van; Beijnen, J. H.; Schellens, J. H. M. *Cancer Chemother. Pharmacol.* **2004**, 54, 71-78.
[36] Lipponer, K.-G.; Vogel, E.; Keppler, B. K. *Metal-Based Drugs* **1996**, 3, 243-260.
[37] Trondl, R.; Heffeter, P.; Kowol, C. R.; Jakupec, M. A.; Berger, W.; Keppler, B. K. *Chem. Sci.* **2014**, 5, 2925-2932.
[38] Clarke, M. J. *Coord. Chem. Rev.* **2002**, 232, 69-93.
[39] Aird, R. E.; Cummings, J.; Ritchie, A. A.; Muir, M.; Morris, R. E.; Chen, H.; Sadler, P. J.; Jodrell, D. I. *Br. J. Cancer* **2002**, 86, 1652-1657.
[40] Scolaro, C.; Bergamo, A.; Brescacin, L.; Delfino, R.; Cocchietto, M.; Laurenczy, G.; Geldbach, T. J.; Sava, G.; Dyson, P. J. *J. Med. Chem.* **2005**, 48, 4161-4171.
[41] Ronconi, L.; Sadler, P. J. *Coord. Chem. Rev.* **2007**, 251, 1633-1648.
[42] Rostovtsev, V. V.; Green, L. G.; Fokin, V. V.; Sharpless, K. B. *Angew. Chem. Int. Ed.* **2002**, 41, 2596-2599.
[43] Tornøe, C. W.; Christensen, C.; Meldal, M. *J. Org. Chem.* **2002**, 67, 3057-3064.
[44] Kolb, H. C.; Finn, M. G.; Sharpless, K. B. *Angew. Chem. Int. Ed.* **2001**, 40, 2004-2021.
[45] Agalave, S. G.; Maujan, S. R.; Pore, V. S. *Chem. Asian J.* **2011**, 6, 2696-2718.
[46] Bock, V. D.; Speijer, D.; Hiemstra, H.; Maarseveen, J. H. van. *Org. Biomol. Chem.* **2007**, 5, 971-975.
[47] Da Silva, F. de C.; de Souza, M. C. B. V.; Frugulhetti, I. I. P.; Castro, H. C.; Souza, S. L. de O.; de Souza, T. M. L.; Rodrigues, D. Q.; Souza, A. M. T.; Abreu, P. A.; Passamani, F.; Rodrigues, C. R.; Ferreira, V. F. *Eur. J. Med. Chem.* **2009**, 44, 373-383.
[48] Dabak, K.; Sezer, Ö.; Akar, A.; Anaç, O. *Eur. J. Med. Chem.* **2003**, 38, 215-218.
[49] Pagliai, F.; Pirali, T.; Del Grosso, E.; Di Brisco, R.; Tron, G. C.; Sorba, G.; Genazzani, A. A. *J. Med. Chem.* **2005**, 49, 467-470.
[50] Lee, T.; Cho, M.; Ko, S.-Y.; Youn, H.-J.; Baek, D. J.; Cho, W.-J.; Kang, C.-Y.; Kim, S. *J. Med. Chem.* **2007**, 50, 585-589.
[51] Kallander, L. S.; Lu, Q.; Chen, W.; Tomaszek, T.; Yang, G.; Tew, D.; Meek, T. D.; Hofmann, G. A.; Schulz-Pritchard, C. K.; Smith, W. W.; Janson, C. A.; Ryan, M. D.; Zhang, G.-F.; Johanson, K. O.; Kirkpatrick, R. B.; Ho, T. F.; Fisher, P. W.; Mattern, M. R.; Johnson, R. K.; Hansbury, M. J.; Winkler, J. D.; Ward, K. W.; Veber, D. F.; Thompson, S. K. *J. Med. Chem.* **2005**, 48, 5644-5647.
[52] Vantikommu, J.; Palle, S.; Surendra Reddy, P.; Ramanatham, V.; Khagga, M.; Pallapothula, V. R. *Eur. J. Med. Chem.* **2010**, 45, 5044-5050.
[53] Schinkel, M.; Marek, I.; Ackermann, L. *Angew. Chem. Int. Ed.* **2013**, 52, 3977-3980.
[54] Ackermann, L.; Vicente, R.; Althammer, A. *Org. Lett.* **2008**, 10, 2299-2302.
[55] Ackermann, L.; Born, R.; Vicente, R. *ChemSusChem* **2009**, 2, 546-549.
[56] Ackermann, L.; Vicente, R.; Potukuchi, H. K.; Pirovano, V. *Org. Lett.* **2010**, 12, 5032-5035.
[57] Yang, F.; Ackermann, L. *J. Org. Chem.* **2014**, 24, 12070-12082.

[58] Zhang, L.; Li, L.-H.; Wang, Y.-Q.; Yang, Y.-F.; Liu, X.-Y.; Liang, Y.-M. *Organometallics* **2014**, 33, 1905-1908.
[59] Vougioukalakis, G. C.; Grubbs, R. H. *Chem. Rev.* **2010**, 110, 1746-1787.
[60] Liu, W.; Gust, R. *Chem. Soc. Rev.* **2012**, 42, 755-773.
[61] Gautier, A.; Cisnetti, F. *Metallomics* **2012**, 4, 23-32.
[62] Oehninger, L.; Alborzinia, H.; Ludewig, S.; Baumann, K.; Wölfl, S.; Ott, I. *ChemMedChem* **2011**, 6, 2142-2145.
[63] Mathew, P.; Neels, A.; Albrecht, M. *J. Am. Chem. Soc.* **2008**, 130, 13534-13535.
[64] Kilpin, K. J.; Crot, S.; Riedel, T.; Kitchen, J. A.; Dyson, P. J. *Dalton Trans.* **2014**, 43, 1443-1448.
[65] Yuan, D.; Huynh, H. V. *Organometallics* **2011**, 31, 405-412.
[66] Liang, L.; Astruc, D. *Coord. Chem. Rev.* **2011**, 255, 2933-2945.
[67] Ahlquist, M.; Fokin, V. V. *Organometallics* **2007**, 26, 4389-4391.
[68] Hein, J. E.; Fokin, V. V. *Chem. Soc. Rev.* **2010**, 39, 1302-1315.
[69] Alvarez, S. G.; Alvarez, M. T. *Synthesis* **1997**, 4, 413.
[70] Kolb, H. C.; Finn, M. G.; Sharpless, K. B. *Angew. Chem. Int. Ed.* **2001**, 40, 2004.
[71] Kacprzak, K. *Synlett* **2005**, 6, 943-946.
[72] Schmidlehner, M.; Pichler, V.; Roller, A.; Jakupec, M. A.; Kandioller, W.; Keppler, B. K. *J. Organomet. Chem.*, in press.
[73] Hameka, H. F. *J. Org. Chem.* **1987**, 52, 5025-5016.
[74] Janiak, C. J. Chem. Soc., *Dalton Trans.* **2000**, 21, 3885-3896.

CURRICULUM VITAE

Personal information

First name / Surname	Christoph Riedl B.Sc.
Address	Froehlerweg 37, 4040 Linz, Austria
Mobile	+43 676 63 55 848
E-Mail	christoph.riedl@univie.ac.at
Date of birth	04.04.1991
Nationality	Austria

Education

05/2013 – ongoing	Master program Chemistry, University of Vienna Qualification: Master of Science (M.Sc.)
10/2009 – 05/2013	Bachelor program Chemistry, University of Vienna Qualification: Bachelor of Science (B.Sc.), passed with distinction
09/2001 – 06/2009	Bischöfliches Gymnasium Petrinum Linz, Austria Qualification: Matura (A-Levels), passed with distinction
09/1997 – 06/2001	Volksschule Berta von Suttner, Linz (primary school)

Research experience

04/2014 – 02/2015	Master thesis at the University of Vienna: 1,4-Disubstituted 1,2,3-triazoles as novel ligand scaffold for the development of organometallic anticancer agents
08/2013 – 01/2014	Erasmus exchange semester at the University of Lund (Sweden): Design, synthesis and biological characterization of selective Cathepsin-L inhibitors
04/2013 – 06/2013	Bachelor thesis at the University of Vienna: Diastereoselective synthesis of N-chiral (*R*,*R*)- tartaric acid derivatives as potential phase transfer catalysts

Scholarships

2014	Erasmus exchange scholarship
2012, 2011, 2010	Scholarship for academic excellence University of Vienna

Work experience

03/2013 – 06/2013	Tutor: Organic chemistry lab course - University of Vienna
10/2012 – 01/2013	Tutor: Organic chemistry lab course - University of Vienna
08/2011	Internship: Borealis Polyolefine GmbH, Linz – Analytical laboratories
08/2009	Internship: KE Kelit, Linz – Production
08/2007	Internship: KE Kelit, Linz – Production

Language Skills

Mother tongue	German
Excellent knowledge	English
Good knowledge	French, Spanish, Latin

Computer skills Excellent command of Microsoft Office